Probing charged Higgs bosons in the two-Higgs-doublet model type II with vectorlike quarks

R. Benbrik,[1,*] M. Boukidi,[1,†] and S. Moretti[2,3,‡]

[1]*Polydisciplinary Faculty, Laboratory of Fundamental and Applied Physics, Cadi Ayyad University, Sidi Bouzid, B.P., 4162 Safi, Morocco*

[2]*Department of Physics and Astronomy, Uppsala University, Box 516, SE-751 20 Uppsala, Sweden*

[3]*School of Physics and Astronomy, University of Southampton, Southampton SO17 1BJ, United Kingdom*

(Received 18 December 2023; accepted 5 February 2024; published 12 March 2024)

We study the phenomenology of charged Higgs bosons ($H^{\pm}$) and vectorlike quarks (VLQs), denoted as T, the latter possessing a charge identical to the top quark one, within the framework of the two-Higgs-doublet model type II (2HDM-II). Upon examining two scenarios, one featuring a singlet (T) [2HDM-II + (T)] and another a doublet (TB) [2HDM-II + (TB)], we discover that the presence of VLQs has a significant effect on the (pseudo)scalar sector of the 2HDM-II. In particular, this leads to a reduction in the strict constraint on the mass of the charged Higgs boson, which is imposed by B-physics observables, specifically $B \to X_s\gamma$. The observed reduction stems from modifications in the charged Higgs couplings to the Standard Model top and bottom quarks. Notably, the degree of this reduction varies distinctly between the singlet 2HDM+(T) and doublet 2HDM + (TB) scenarios. Additionally, our investigation extends to constraints imposed by the oblique parameters S and T on the VLQ mixing angles. Furthermore, to facilitate efficient exploration of the "2HDM-II + VLQ" parameter space, we present results on pair production of VLQs T ($pp \to T\bar{T}$), followed by $T \to H^{\pm}b$ and $H^{\pm} \to tb$ decays, yielding a distinctive $2t4b$ final state. This investigation thus provides valuable insights guiding the search for extended Higgs and quark sectors at the Large Hadron Collider (LHC) at CERN.

DOI: 10.1103/PhysRevD.109.055016

I. INTRODUCTION

Evidence of either a light or heavy charged spin-0 boson, $H^{\pm}$, with a fundamental (i.e., pointlike) structure would be a crucial piece of evidence suggesting physics beyond the Standard Model (BSM), as such a state would not replicate any of those existing within the SM. The latter, in fact, includes charged bosons, but these are spin-1. Conversely, it includes a spin-0 boson, but this is chargeless. As a consequence, the search for charged Higgs bosons in recent years has received a great boost at existing accelerator machines like the Large Hadron Collider (LHC) at CERN. However, despite all the efforts being made, still no $H^{\pm}$ signals have been seen. Thus, data from direct $H^{\pm}$ searches from both the ATLAS and CMS experiments have excluded large areas of the parameter spaces pertaining to BSM scenarios incorporating these new states. In particular, this has been done for a two-Higgs-doublet model type II (2HDM-II), including its supersymmetric incarnation, the minimal supersymmetric Standard Model (MSSM). However, while the latter is able to escape LHCb indirect limits on $H^{\pm}$ states via, chiefly, $b \to s\gamma$ driven decays of B mesons [thanks to new (s)particles in the corresponding loops canceling the $H^{\pm}$ contributions], this is not possible for the former. Therefore, in the 2HDM-II, a rather stringent lower limit applies on its mass, $m_{H^{\pm}}$, of 580 GeV or so, quite irrespectively of the other model parameters.

Such a constraint can, however, be lifted if the 2HDM-II is supplemented with additional objects flowing inside the loops, enabling the $b \to s\gamma$ transitions, similarly to what happens in the MSSM. The purpose of this paper is to investigate whether a similar phenomenon can be triggered by the presence of vectorlike quarks (VLQs) alongside the particle states of the 2HDM-II. VLQs are (heavy) spin-1/2 states that transform as triplets under color, but, differently from the SM quarks, their left- and right-handed (LH and RH) couplings have the same electroweak (EW) quantum numbers. They are predicted by several theoretical constructs: e.g., models with a gauged flavor group [1–4], nonminimal supersymmetric scenarios [5–10], grand unified

*r.benbrik@uca.ac.ma
†mohammed.boukidi@ced.uca.ma
‡stefano.moretti@physics.uu.se, s.moretti@soton.ac.uk

theories [11,12]), little Higgs [13,14] and composite Higgs [15–22] models, to name but a few. In most of these frameworks, VLQs appear as partners of the third generation of quarks, mixing with top and bottom quarks. Further, if their mass is not exceedingly large for the LHC kinematic reach, they can be accessible in its detectors in a variety of final states [23–27], so that some of these have already been explored by the ATLAS and CMS collaborations [28–52].

Here, rather than invoking a complete theoretical scenario embedding VLQs (like, e.g., compositeness), we adopt a simplified approach by manually extending the 2HDM-II with two VLQ representations (singlet and doublet), in the spirit of Refs. [27,53–57], i.e., for the purpose of assessing the phenomenological consequences of such modifications in general, irrespectively of the underlying theory. Indeed, we will be able to prove that the VLQ loops entering $b \to s\gamma$ transitions can cancel the large contributions due to $H^\pm$ ones, thereby reducing the aforementioned limit on $m_{H^\pm}$ down to approximately 200 GeV for the doublet scenario (2HDM $+TB$) and to around 500 GeV in the singlet scenario (2HDM $+ T$). However, we shall see that achieving this reduction relies on large mixing angles, a condition largely contradicted by constraints imposed by the oblique parameters S and T. The focus then will shift to the production of $H^\pm$ states through $pp \to T\bar{T}$ and $T \to H^\pm b$, with $H^\pm \to tb$, resulting in a final state characterized by two top and four bottom quarks ($2t4b$).

The plan of this paper is as follows: The next section is devoted to introduce our 2HDM-II + VLQ framework. Then we proceed to discuss both theoretical and experimental bounds on it. Section IV presents our numerical results for the two chosen VLQ representations in turn, including providing benchmark points (BPs) amenable to further phenomenological investigation aimed at extracting signatures of the 2HDM-II + VLQ scenario at the LHC. Finally, we conclude. (We also have some Appendixes.)

II. MODEL DESCRIPTIONS

In this section, we only provide a brief overview of the 2HDM-II + VLQ realizations that are relevant to our work. Let us begin with recalling the well-known $\mathcal{CP}$-conserving 2HDM scalar potential for two doublet fields (Φ_1, Φ_2) with a discrete $\mathbb{Z}_2$ symmetry, $\Phi_1 \to -\Phi_1$, which is only violated softly by dimension-2 terms [58,59]:

$$\begin{aligned}\mathcal{V} = {} & m_{11}^2 \Phi_1^\dagger \Phi_1 + m_{22}^2 \Phi_2^\dagger \Phi_2 - \left(m_{12}^2 \Phi_1^\dagger \Phi_2 + \text{H.c.}\right) \\ & + \frac{1}{2}\lambda_1 \left(\Phi_1^\dagger \Phi_1\right)^2 + \frac{1}{2}\lambda_2 \left(\Phi_2^\dagger \Phi_2\right)^2 + \lambda_3 \Phi_1^\dagger \Phi_1 \Phi_2^\dagger \Phi_2 \\ & + \lambda_4 \Phi_1^\dagger \Phi_2 \Phi_2^\dagger \Phi_1 + \left[\frac{1}{2}\lambda_5 \left(\Phi_1^\dagger \Phi_2\right)^2 + \text{H.c.}\right]. \end{aligned} \tag{1}$$

Here, all parameters are real. The two complex scalar doublets $\Phi_{1,2}$ may be rotated into a basis, $H_{1,2}$, where only one obtains a vacuum expectation value (VEV). Using the minimization conditions of the potential for the implementation of EW symmetry breaking (EWSB), the 2HDM can be fully described in terms of seven independent parameters: $m_h, m_H, m_A, m_{H^\pm}, \tan\beta (= v_2/v_1), \sin(\beta - \alpha)$ and the soft breaking parameter m_{12}^2. When we impose that no (significant) tree-level flavor changing neutral currents (FCNCs) are present in the theory, four Yukawa versions of the 2HDM can then be realized, depending on how the $\mathbb{Z}_2$ symmetry is implemented into the fermion sector. These are: type I, where only Φ_2 couples to all fermions; type II, where Φ_2 couples to up-type quarks and Φ_1 couples to charged leptons and down-type quarks; type Y (or flipped), where Φ_2 couples to charged leptons and up-type quarks and Φ_1 couples to down-type quarks; type X (or lepton specific), where Φ_2 couples to quarks and Φ_1 couples to charged leptons.[1]

TABLE I. Singlet and doublet VLQ representations under the SM gauge group.

Component fields	(T)	(TB)
$U(1)_Y$	2/3	1/6
$SU(2)_L$	1	2
$SU(3)_C$	3	3

We now move on to discuss the VLQ side of the model and we start by listing the representations of two gauge-covariant multiplets [(T) and (TB)] in Table I, where the fields T and B have electric charges 2/3 and $-1/3$, respectively. Specifically, the T is chosen as triplet under the color group $SU(3)_C$ and singlet under the EW group $SU(2)_L \times U(1)_Y$. Furthermore, the RH and LH components $T_{L,R}^0$ have the same EW and color quantum numbers. The mixing of VLQs with the first and second generations of SM quarks is heavily constrained by low energy physics measurement constraints. One such example of such constraints originates from the EW precision observables (EWPOs), including oblique parameter corrections, these being radiative corrections to quantities such as the $W^\pm$ boson mass $(m_{W^\pm})$ and to the effective mixing angle $(\sin^2\theta_W)$ at high orders [60,61]. Such corrections may be sensitive to VLQs and may impose restrictions on their masses and couplings. Additionally, as mentioned, VLQs, especially the third generation, may also affect the properties of top and bottom quarks through the mixing of fermions [62]. This may have implications for processes like the decay of the Z boson into bottom quarks, which were measured with high precision at the LEP e^+e^- collider at energies near the Z resonance [63,64]. Deviations from SM predictions in such measurements have the potential to provide strong constraints on the

[1]In this paper, we will be discussing only type II.

properties of VLQs. We thus focus on scenarios in which the VLQs interact solely to third-generation SM quarks.

In the Higgs basis, the Yukawa Lagrangian can be written as

$$-\mathcal{L} \supset y^u \bar{Q}_L^0 \tilde{H}_2 u_R^0 + y^d \bar{Q}_L^0 H_1 d_R^0 + M_u^0 \bar{u}_L^0 u_R^0 + M_d^0 \bar{d}_L^0 d_R^0 + \text{H.c.} \tag{2}$$

Here, u_R actually runs over (u_R, c_R, t_R, T_R) and d_R actually runs over (d_R, s_R, b_R, B_R) while $y^{u,d}$ are 3×4 Yukawa matrices. When only the top quark "mixes" with T, the relation between mass eigenstates $(T_{L,R})$ and weak eigenstates $(T_{L,R}^0)$ can be factored into two 2×2 unitary matrices $U_{L,R}$, such that

$$\begin{aligned}\begin{pmatrix} t_{L,R} \\ T_{L,R} \end{pmatrix} &= U_{L,R}^u \begin{pmatrix} t_{L,R}^0 \\ T_{L,R}^0 \end{pmatrix} \\ &= \begin{pmatrix} \cos\theta_{L,R}^u & -\sin\theta_{L,R}^u e^{i\phi_u} \\ \sin\theta_{L,R}^u e^{-i\phi_u} & \cos\theta_{L,R}^u \end{pmatrix} \\ &\quad \times \begin{pmatrix} t_{L,R}^0 \\ T_{L,R}^0 \end{pmatrix}, \end{aligned} \tag{3}$$

where θ is the mixing angle between mass and weak eigenstates and ϕ is a possible $\mathcal{CP}$-violating phase which will be ignored in our work. In the weak eigenstate basis, the diagonalization of the mass matrices makes the Lagrangian of the third generation and heavy quark mass terms such that

$$\begin{aligned}\mathcal{L}_{\text{mass}} = &-\begin{pmatrix} \bar{t}_L^0 & \bar{T}_L^0 \end{pmatrix} \begin{pmatrix} y_{33}^u \frac{v}{\sqrt{2}} & y_{34}^u \frac{v}{\sqrt{2}} \\ y_{43}^u \frac{v}{\sqrt{2}} & M^0 \end{pmatrix} \begin{pmatrix} t_R^0 \\ T_R^0 \end{pmatrix} \\ &- \begin{pmatrix} \bar{b}_L^0 & \bar{B}_L^0 \end{pmatrix} \begin{pmatrix} y_{33}^d \frac{v}{\sqrt{2}} & y_{34}^d \frac{v}{\sqrt{2}} \\ y_{43}^d \frac{v}{\sqrt{2}} & M^0 \end{pmatrix} \begin{pmatrix} b_R^0 \\ B_R^0 \end{pmatrix} \\ &+ \text{H.c.}, \end{aligned} \tag{4}$$

where M^0 is a bare mass and the y_{ij}'s are Yukawa couplings. For the singlet case $y_{43} = 0$, while for the doublet one has $y_{34} = 0$. Using standard techniques of diagonalization, the mixing matrices are obtained by

$$U_L^q \mathcal{M}^q (U_R^q)^\dagger = \mathcal{M}_{\text{diag}}^q, \tag{5}$$

with $\mathcal{M}^q$ the two mass matrices in Eq. (4) and $\mathcal{M}_{\text{diag}}^q$ the diagonalized ones. The mixing angles in the LH and RH sectors are not independent parameters. Using Eq. (5) and depending on the VLQs representation, one can find

$$\begin{aligned}\tan\theta_R^q &= \frac{m_q}{m_Q} \tan\theta_L^q \quad \text{(singlet)}, \\ \tan\theta_L^q &= \frac{m_q}{m_Q} \tan\theta_R^q \quad \text{(doublet)}, \end{aligned} \tag{6}$$

with $(q, m_q, m_Q) = (u, m_t, m_T)$ and (d, m_b, m_B).

III. THEORETICAL AND EXPERIMENTAL BOUNDS

In this section, we list the constraints that we have used to check the validity of our results. From the theoretical side, we have the following requirements:

(i) *Unitarity* constraints require the S-wave component of the various (pseudo)scalar-(pseudo)scalar, (pseudo)scalar-gauge boson, and gauge-gauge bosons scatterings to be unitary at high energy [65].

(ii) *Perturbativity* constraints impose the following condition on the quartic couplings of the scalar potential: $|\lambda_i| < 8\pi$ $(i = 1, \ldots 5)$ [58].

(iii) *Vacuum stability* constraints require the potential to be bounded from below and positive in any arbitrary direction in the field space; as a consequence, the λ_i parameters should satisfy the conditions as [66,67]

$$\begin{aligned}&\lambda_1 > 0, \qquad \lambda_2 > 0, \qquad \lambda_3 > -\sqrt{\lambda_1 \lambda_2}, \\ &\lambda_3 + \lambda_4 - |\lambda_5| > -\sqrt{\lambda_1 \lambda_2}. \end{aligned} \tag{7}$$

(iv) *Constraints from EWPOs*, implemented through the oblique parameters,[2] S and T [70], require that, for a parameter point of our model to be allowed, the corresponding $\chi^2(S^{\text{2HDM-II}} + S^{\text{VLQ}}, T^{\text{2HDM-II}} + T^{\text{VLQ}})$ is within 95% confidence level (CL) in matching the global fit results [71]:

$$\begin{aligned}&S = 0.05 \pm 0.08, \qquad T = 0.09 \pm 0.07, \\ &\rho_{S,T} = 0.92 \pm 0.11. \end{aligned}$$

Note that unitarity, perturbativity, vacuum stability, as well as S and T constraints, are enforced through the public code 2HDMC-1.8.0[3] [72].

From the experimental side, we evaluated the following:

(1) *Constraints from the SM-like Higgs-boson properties* are taken into account by using HIGGSSIGNAL-3 [73,74] via HIGGSTOOLS [75]. We require that the relevant quantities (signal strengths, etc.) satisfy

[2]To compute the S and T parameters for the VLQ representations investigated in this study, we employed dimensional regularization by employing the FEYNARTS and FORMCALC packages [68,69].

[3]The code has been adjusted to include new VLQ couplings, along with the integration of analytical expressions for S_{VLQs} and T_{VLQs} outlined in Appendix C.

TABLE II. Yukawa couplings of the charged Higgs bosons $H^{\pm}$ to the third generation of quarks in the 2HDM-II and 2HDM-II + VLQ representations studied here [(T) and (TB)]. Here $s_{L,R} = \sin\theta_{L,R}$ and $c_{L,R} = \cos\theta_{L,R}$.

Models	κ_t	κ_b
2HDM-II	$\cot\beta$	$-\tan\beta$
2HDM-II + (T)	$c_L \cot\beta$	$-c_L \tan\beta$
2HDM-II + (TB)	$\cot\beta\left[c_L^d c_L^u + \frac{s_L^d}{s_L^u}(s_L^{u\,2} - s_R^{u\,2})e^{i(\phi_u-\phi_d)}\right]$	$-\tan\beta\left[c_L^u c_L^d + \frac{s_L^u}{s_L^d}(s_L^{d\,2} - s_R^{d\,2})e^{i(\phi_u-\phi_d)}\right]$

$\Delta\chi^2 = \chi^2 - \chi^2_{\rm min}$ for these measurements at 95% CL ($\Delta\chi^2 \leq 6.18$).

(2) *Constraints from direct searches at colliders*, i.e., LEP, Tevatron, and LHC, are taken at the 95% CL and are tested using HiggsBounds-6 [76–79] via HiggsTools. Including the most recent searches for neutral and charged scalars.

(3) *Constraints from flavor physics* are taken at 95% CL from experimental measurements and are accounted for via the public code SuperIso_v4.1 [80]. Specifically, we have used the following measurements for the most relevant branching ratios ($\mathcal{BR}$s):
   (a) $\mathcal{BR}(\bar{B} \to X_s\gamma)|_{E_\gamma < 1.6\,\text{GeV}} = (3.32 \pm 0.15) \times 10^{-4}$ [81],
   (b) $\mathcal{BR}(B^+ \to \tau^+\nu_\tau) = (1.06 \pm 0.19) \times 10^{-4}$ [81],
   (c) $\mathcal{BR}(B_s \to \mu^+\mu^-) = (3.83^{+0.38}_{-0.36}) \times 10^{-9}$ [82],
   (d) $\mathcal{BR}(B^0 \to \mu^+\mu^-) = (1.2^{+0.8}_{-0.7}) \times 10^{-10}$ [83,84].

IV. NUMERICAL RESULTS

In this section, we present our numerical results by first describing the Lagrangian terms relevant to $b \to s\gamma$ transitions in the 2HDM-II + VLQ scenarios considered, then by characterizing the implications of the latter in the case of the (T) and (TB) representations chosen here in turn, and, finally, by presenting some BPs amenable to experimental investigation.

A. Charged Higgs boson contributions to flavor observables

In the following, we shall discuss the results of the most relevant B-physics constraints, from $b \to s\gamma$ transitions, onto the 2HDM-II + VLQ scenarios considered.

The Lagrange density, which defines the interactions of the charged Higgs boson with third generation fermions, can be written as

$$-\mathcal{L}_{H^+} = \frac{\sqrt{2}}{v}\bar{t}(\kappa_t m_t P_L - \kappa_b m_b P_R) b H^+ + \text{H.c.}, \quad (8)$$

where $P_{L/R} = (1 \pm \gamma^5)/2$ are the chiral projection operators. For the 2HDM-II, 2HDM-II + (T), and 2HDM-II + (TB) cases, the couplings κ_t and κ_b take the values presented in Table II. We emphasize here the role of the Yukawa couplings, as it is the changes of the latter occurring in the presence of VLQs which are responsible for the forthcoming results, as opposed to the role of the VLQs in the loop observables that we will be describing, owing to the far too large values of their masses (of order 750 GeV or more).

The Table summarizes the Yukawa couplings of charged Higgs bosons to quarks of the third generation for three distinct representations: 2HDM-II, 2HDM-II + (T), and 2HDM-II + (TB), providing insights into the modification patterns in different scenarios. As indicated, the couplings of the charged Higgs boson to SM quarks, specifically to the top (t) and bottom (b), undergo modifications in both VLQ representations.[4] These alterations lead to significant changes in observables related to B-physics processes, such as $b \to s\gamma$ and $B_{s/d} \to \mu^+\mu^-$. The contributions to the corresponding Wilson coefficients ($C_{7,8}$) are proportional to $\kappa_i\kappa_j^*$, where the terms can be further decomposed into two parts. Detailed expressions of $C^t_{i,\kappa_b\kappa_t^*}$ can be found in Ref. [85].

The contributions[5] to $C_i^{t,\text{model}}$ take the form

$$C_i^{t,\text{model}} = \kappa_b\kappa_t^* C^{t,\text{model}}_{i,\kappa_b\kappa_t^*} + \kappa_t\kappa_t^* C^{t,\text{model}}_{i,\kappa_t\kappa_t^*}. \quad (9)$$

The outcomes of these modifications will be presented in the following subsections.

B. 2HDM-II + (T)

We start with Fig. 1, where we present explicitly the excluded parts of the $(m_{H^\pm}, \tan\beta)$ plane at 95% CL by $\bar{B} \to X_s\gamma$ (hatched areas) alongside $B_d^0 \to \mu^+\mu^-$ (green), $B_s^0 \to \mu^+\mu^-$ (orange, which is hardly visible in the plots), and $B_u \to \tau\nu$ (blue). This figure illustrates that higher values of s_L lead to a less stringent constraint from $B \to X_s\gamma$, driving the exclusion regions towards smaller values of the charged Higgs boson mass, reaching approximately $m_{H^\pm} \simeq 500$ GeV for $s_L = 0.45$. Conversely, the limits from

[4]For the detailed analytic calculation of charged Higgs boson couplings, please refer to Appendix A.

[5]In this study, we neglect contributions from Feynman diagrams involving VLQs, focusing solely on diagrams that involve SM quarks. This deliberate exclusion stems from the observation that the impact of VLQ diagrams is negligible when contrasted with the diagrams incorporating SM quarks.

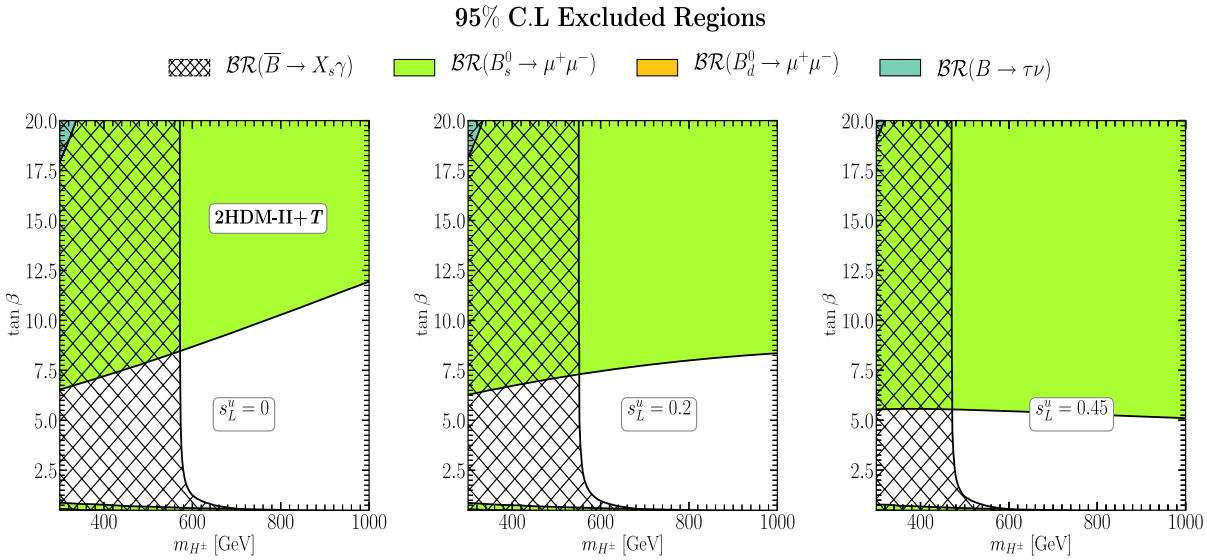

FIG. 1. Excluded regions of the $(m_{H^\pm}, \tan\beta)$ parameter space by flavor constraints at 95% CL. Plots are presented for the 2HDM-II + (T) singlet with $s_L^u = 0$ (left), $s_L^u = 0.2$ (middle), and $s_L^u = 0.45$ (right).

$B_s \to \mu^+\mu^-$ become more restrictive as s_L increases, excluding $\tan\beta \lesssim 7$ for $s_L = 0.25$ and $\tan\beta \lesssim 5$ for $s_L = 0.45$. Here, it is important to note that the new term introduced in the relevant $H^\pm tb$ coupling depends solely on the mixing angle s_L, which thus controls the inclusion of VLQs in the 2HDM-II, as discussed previously.

However, the potential for this reduction is moderated by the oblique parameters S and T, as will be discussed subsequently. These parameters restrict the range of the mixing angle s_L, thereby playing a critical role in preventing a substantial decrease in the charged Higgs mass limit, particularly by constraining the possibility of larger mixing angles.

In Fig. 2, we show the result of the analysis for our scan over the (S, T) plane. The color coding indicates the difference with respect to the $\chi^2(S, T)$ values, and the black lines show the 68% CL (solid) and 95% CL (dashed) contours. The scanned 2HDM-II + VLQ parameters[6] are given in Table III. In the remainder of our analysis, we will present results from the 2HDM-II + (T) regions within the 2σ band also compliant with flavor constraints. It is important to highlight that the shape of these points is a result of the cancellation between the contributions from the 2HDM and VLQ states to the oblique parameters S and T.

Figure 3 illustrates the excluded regions at 95% CL by S and T in the (m_T, s_L^u) plane, considering the fixed parameters $m_H = 532.80$ GeV, $m_A = 524.26$ GeV, and $m_{H^\pm} = 588.02$, with $\tan\beta = 5.19$. From this figure, it is evident that the imposed constraints only permit low mixing angles,

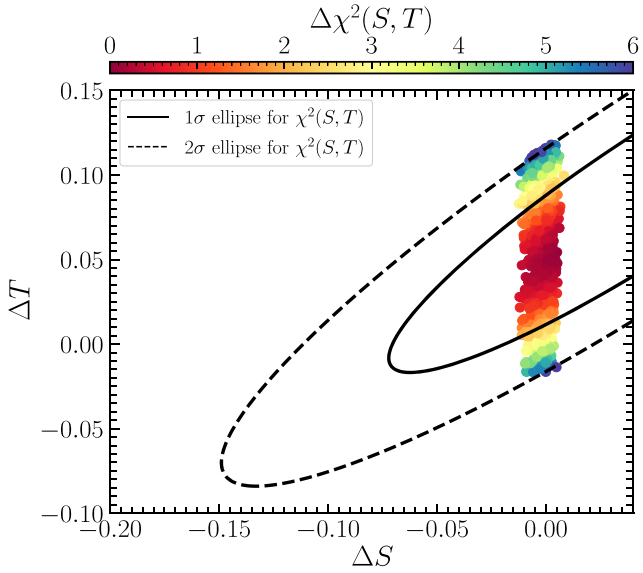

FIG. 2. Allowed points by all constraints (HIGGSBOUNDS, HIGGSSIGNALS, SUPERISO, and theoretical ones) superimposed onto the fit limits in the (S, T) plane from EWPO data at 95% CL (with a correlation of 92%), with the color code indicating $\Delta\chi^2(S, T)$. Results are presented for the 2HDM-II + (T).

specifically $s_L^u \lesssim 0.1$. Additionally, the stringency of the constraint increases with rising VLQ mass, m_T.

In Fig. 4, we illustrate the $\mathcal{BR}(T \to H^+ b)$ (left) and the ratio Γ_T/m_T (right) as a function of m_T and $\tan\beta$. It is clear from the left plot that the 2HDM-II + (T) scenario cannot ultimately predict dominant production rates for a $H^\pm$ emerging from a heavy T quark, no matter its final decay pattern. Specifically, the decay rate of $T \to H^\pm b$ reaches a maximum value of 23% for $\tan\beta \leq 1.5$ and

[6]We performed a systematic random scan over the parameters cited in Table III using a modified version of 2HDMC-1.8.0.

TABLE III. 2HDM and VLQs parameters with their scanned ranges for both VLQ representations considered here. Masses are in GeV. (Note that we have taken the lightest $\mathcal{CP}$-even neutral Higgs boson, h, to be the one observed at ∼125 GeV).

Parameters	Scanned ranges
2HDM	
m_H	[130, 800]
m_A	[80, 800]
$m_{H^\pm}$	[80, 800]
$\tan\beta$	[0.5, 20]
$\sin(\beta-\alpha)$	1
2HDM-II + (T)	
s_L	[−0.5, 0.5]
m_T	[750, 2600]
2HDM-II + (TB)	
$s_R^{u,d}$	[−0.5, 0.5]
m_T	[750, 2600]

$m_T \geq 1500$ GeV and becomes negligible for $\tan\beta \geq 4$, essentially due to the dependence of the $\mathcal{BR}$ on the mixing angle s_L. Recall, in fact, that the latter is constrained to be rather small by the oblique parameters S and T. One can also read from the right panel of the figure that the heavy quark total width can be at most 10% of its mass at low $\tan\beta$ (indicated by dark blue points), so that this state is generally rather narrow and then can (tentatively, depending on the $H^\pm$ decays) be reconstructed in LHC analysis.

We then present in Fig. 5 the $\mathcal{BR}^2(T \to H^+ b) \times \mathcal{BR}^2(H^+ \to t\bar{b})$ (left) and the production cross section $\sigma(pp \to T\bar{T})$[7] followed by $\mathcal{BR}^2(T \to H^+ b)$ and $\mathcal{BR}^2(H^+ \to t\bar{b})$ in the $(m_T, m_{H^\pm})$ plane. Clearly from the left panel, the decay $H^+ \to t\bar{b}$ as this is the dominant one for a heavy $H^\pm$ state with $m_{H^\pm} > m_t$. In the left panel, $\mathcal{BR}^2(T \to H^+ b) \times \mathcal{BR}^2(H^+ \to t\bar{b})$ reaches around 4% for $\tan\beta \leq 2$ while, in the right panel, $\sigma_{T\bar{T}} \times \mathcal{BR}^2(T \to H^+ b) \times \mathcal{BR}^2(H^+ \to t\bar{b})$ can exceed 0.2 fb for $m_T <$ 1000 GeV and for small $\tan\beta$. The emerging $2t4b$ signal[8] can then potentially be pursued at the LHC [88].

C. 2HDM-II + (TB)

In this section, we discuss the case of the 2HDM-II + (TB). In the SM extended with such a VLQ multiplet, both mixing angles in the up- and down-type quark sectors enter the phenomenology of the model. For a given θ_R^b, θ_R^t, and m_T mass, the relationship between the mass eigenstates and the mixing angles is given by [27]

$$m_B^2 = \left(m_T^2 \cos^2\theta_R^t + m_t^2 \sin^2\theta_R^t - m_b^2 \sin^2\theta_R^b\right)/\cos^2\theta_R^b. \tag{10}$$

Using the above relation, one can then compute m_B for a given m_T and mixing angles θ_R^b and θ_R^t. Additionally, the left mixings θ_L^b, θ_L^t may be calculated using Eq. (6).

In Fig. 6, we once again present the excluded regions over the $(m_{H^\pm}, \tan\beta)$ plane at a 95% CL. The exclusions are derived from $\bar{B} \to X_s\gamma$ (depicted as hatched areas) as well as from $B_d^0 \to \mu^+\mu^-$ (depicted in green), $B_s^0 \to \mu^+\mu^-$ (depicted in orange), and $B_u \to \tau\nu$ (depicted in blue). Notably, in this representation, the limit imposed by $\bar{B} \to X_s\gamma$ can be further diminished compared to the singlet scenario. The exclusions shift the regions for $B \to X_s\gamma$ towards smaller values of the charged Higgs boson mass, particularly reaching $m_{H^\pm} \sim 400$ GeV for $s_R^d = 0.2$ and $m_{H^\pm} \simeq 180$ GeV for $s_R^d = 0.45$, maintaining a fixed value of s_R^u at 0.05 in both cases. Similarly to the previous scenario, the constraints from $B_s \to \mu^+\mu^-$ become more stringent than in the 2HDM case in this representation, excluding all values above $\tan\beta \simeq 5$.

Following the scan described in Table III, we again present in Fig. 7 our 2HDM-II + (TB) surviving points in the (S, T) plane, wherein the color illustrates the usual difference in $\chi^2(S, T)$ values. As previously, we will define the dataset to be used for additional analysis as the one lying within the illustrated 2σ band. As evident, in this representation, the shape differs from the one presented in the previous representation, and this is again attributed to the cancellation of contributions from 2HDM-II and VLQ states to the oblique parameters S and T.

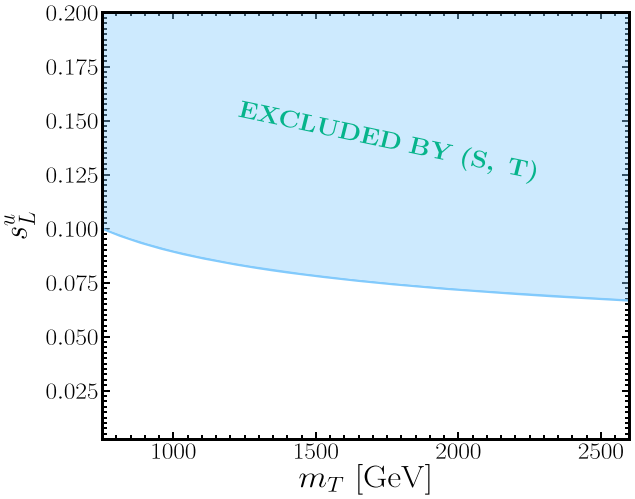

FIG. 3. Exclusion regions by (S, T) in the (m_T, s_R^d) plane with fixed parameters: $m_H = 532.80$, $m_A = 524.26$, and $m_{H^\pm} = 588.02$ GeV, with $\tan\beta = 5.19$.

[7]The cross section $\sigma(pp \to T\bar{T})$ is computed at leading order using MADGRAPH5_AMC@NLO-3.4.0 [86] for $\sqrt{s} = 14$ TeV, with CTEQ6L [87] as the parton distribution functions (PDFs) with default settings.

[8]A similar signal has been investigated within the 2HDM-II + VLQs framework in [88].

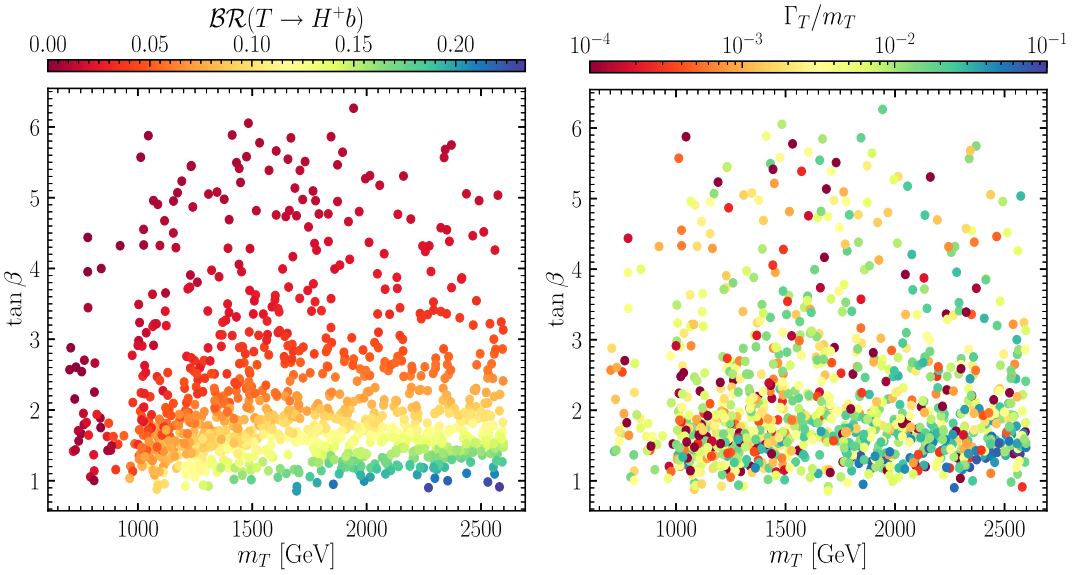

FIG. 4. $\mathcal{BR}(T \to H^+ b)$ (left) and Γ_T/m_T (right) plotted over the $(m_T, \tan\beta)$ plane. Results are presented for the 2HDM-II + (T).

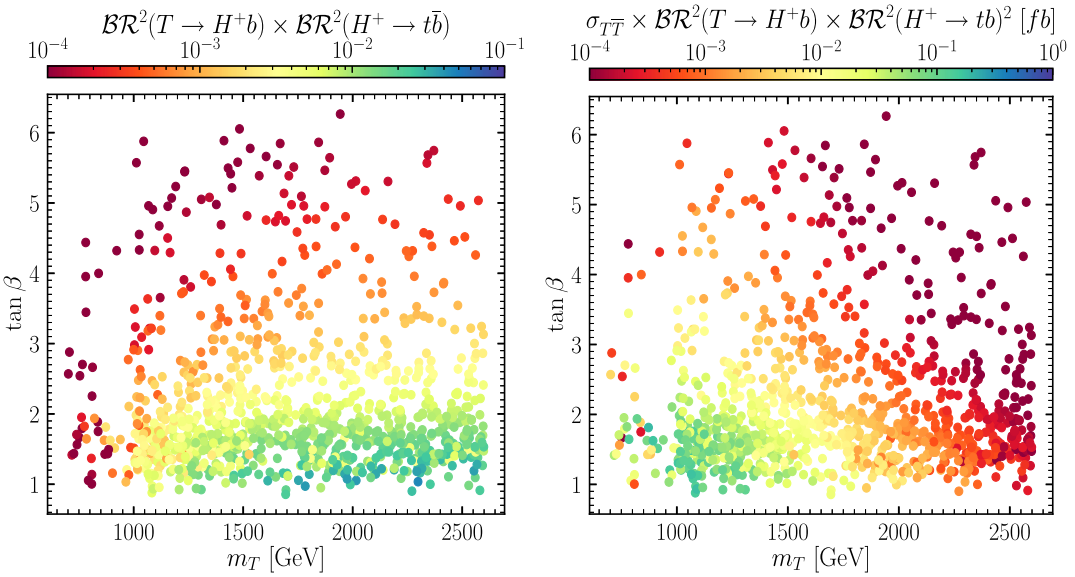

FIG. 5. $\mathcal{BR}^2(T \to H^+ b) \times \mathcal{BR}^2(H^+ \to tb)$ (left) and $\sigma_{T\bar{T}} \times \mathcal{BR}^2(T \to H^+ b) \times \mathcal{BR}^2(H^+ \to tb)$ (right) plotted over the $(m_T, \tan\beta)$ plane. Results are presented for the 2HDM-II + (T). The two selected BPs are highlighted in green stars (see later).

Figure 8 illustrates the exclusion region derived from the oblique parameters S and T at 2σ. It is evident from the plot that EWPOs impose a stringent limit on the mixing angles. Specifically, as the mixing angle s_R^u increases, the exclusion region expands, covering the entire mass range of m_T. Similarly, for the mixing angle s_R^d, an increase in the VLQ mass m_T results in a larger exclusion region.

From Fig. 9 (left), in contrast to the previous VLQ realization, it is clear that charged Higgs boson production from T decays can reach more than 90% in the corresponding $\mathcal{BR}$ for medium $\tan\beta$. In the right plot of the figure, we display Γ_T/m_T as a function of m_T and $\tan\beta$, where it can be seen that the total decay width of the T state can reach 30% of m_T. Hence, unlike the singlet case, here we are normally in the presence of a rather sizable $T \to H^\pm b$ rate, which is affected by phase space effects only for light T states. Conversely, though, the T state can be quite wide, thereby rendering attempts at reconstructing its mass from kinematic analysis potentially more difficult than in the singlet case.

In Fig. 10, we present in the $(m_T, \tan\beta)$ plane the aforementioned distribution of points mapped against

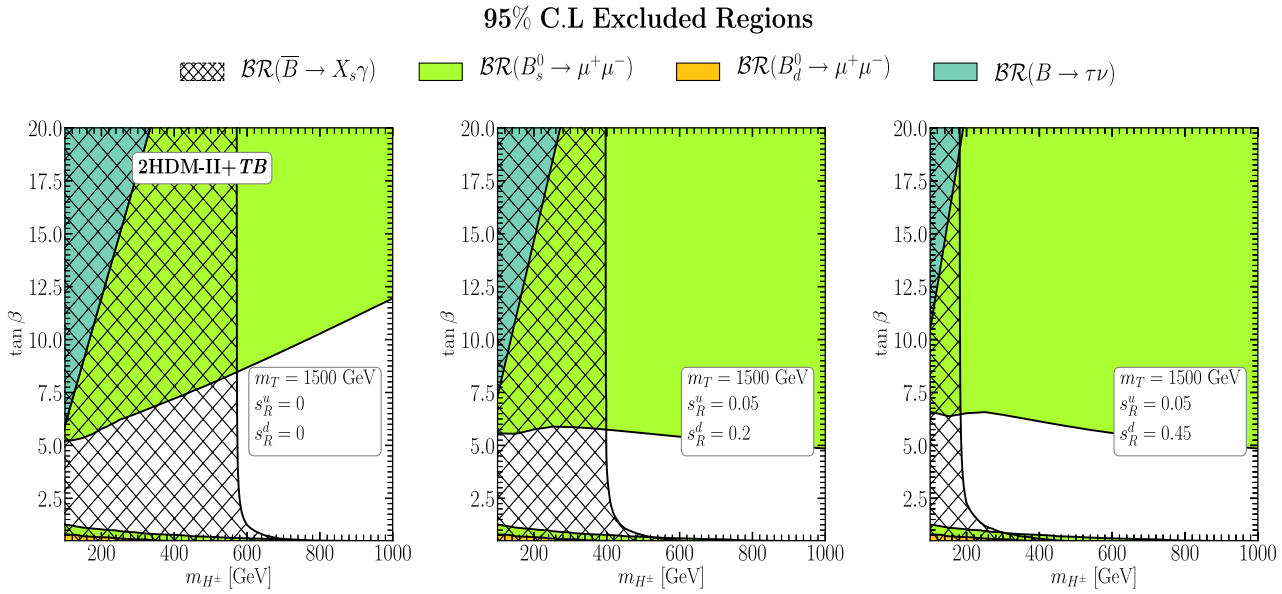

FIG. 6. Excluded regions of the $(m_{H^\pm}, \tan\beta)$ parameter space by flavor constraints at 95% CL. Plots are presented for the 2HDM-II + (TB) doublet with $s_R^d = 0$ (left), $s_R^d = 0.2$ (middle), and $s_R^d = 0.45$ (right), with fixed $s_R^u = 0.05$.

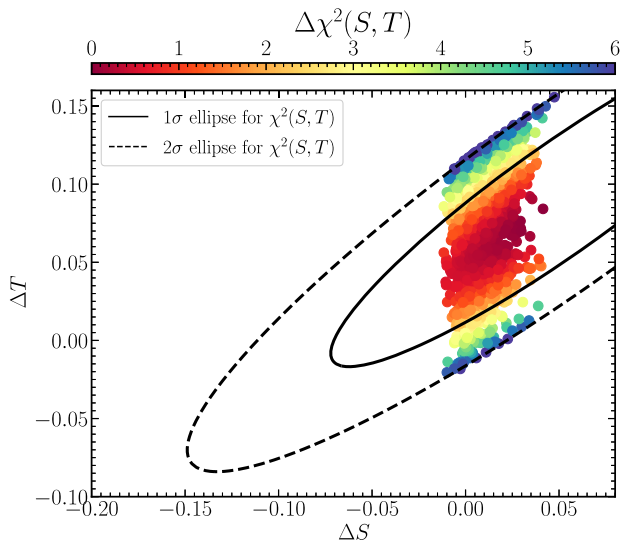

FIG. 7. Allowed points by all constraints (HIGGSBOUNDS, HIGGSSIGNALS, SUPERISO, and theoretical ones) superimposed onto the fit limits in the (S,T) plane from EWPO data at 95% CL (with a correlation of 92%), with the color code indicating $\Delta\chi^2(S,T)$. Results are presented for the 2HDM-II + (TB).

$\mathcal{BR}^2(T \to H^+b) \times \mathcal{BR}^2(H^+ \to tb)$ (left panel) and $\sigma_{T\bar{T}} \times \mathcal{BR}^2(T \to H^+b) \times \mathcal{BR}^2(H^+ \to tb)$ (right panel). One can see from these plots that the signal $2t4b$ could reach values up to 100 fb for medium $\tan\beta$ and for $m_T \leq 1000$ GeV. Therefore, owing to the enhanced coupling TH^+b in this scenario, a much larger cross section is observed for this signature compared to the 2HDM-II + (T) case.

D. BPs

Before concluding, in order to encourage experimental analyses of these scenarios at the LHC, we propose three BPs in Table IV for the 2HDM-II + (TB) representation, which exhibits a more substantial cross section compared to the 2HDM-II + (T) one. The chosen BPs feature T masses within the range of approximately 800 to 1300 GeV. Furthermore, the $H^\pm$ masses are set to be heavy, enabling attempts to extract charged Higgs boson signatures in its tb decay, presenting a significant signal in the form of $2t4b$ final states originating from the pair production of the new VLQ T, followed by $T \to H^+b$ and $H^+ \to tb$ decays.

V. CONCLUSIONS

This paper goes into great detail about how charged Higgs bosons are made with a new top partner T in two different forms: 2HDM-II + (T) (singlet) and 2HDM-II + (TB) (doublet). Our findings reveal a compelling capability of VLQs to alleviate the stringent limit imposed by $B \to X_s\gamma$ on the charged Higgs mass $(m_{H^\pm})$. Specifically, in the singlet scenario, the mass limit can be reduced to around 500 GeV, while in the doublet case, it can decrease to approximately 200 GeV, particularly when the mixing angles are large. However, the inclusion of constraints from the oblique parameters S and T implies additional limitations, allowing only small VLQ mixing angles, in turn somewhat restraining the reduction in the aforementioned limit on $m_{H^\pm}$. Consequently, in the 2HDM-II + (T) scenario, the mass limit decreases to about 567 GeV, and in the 2HDM-II + (TB) scenario, it reduces to

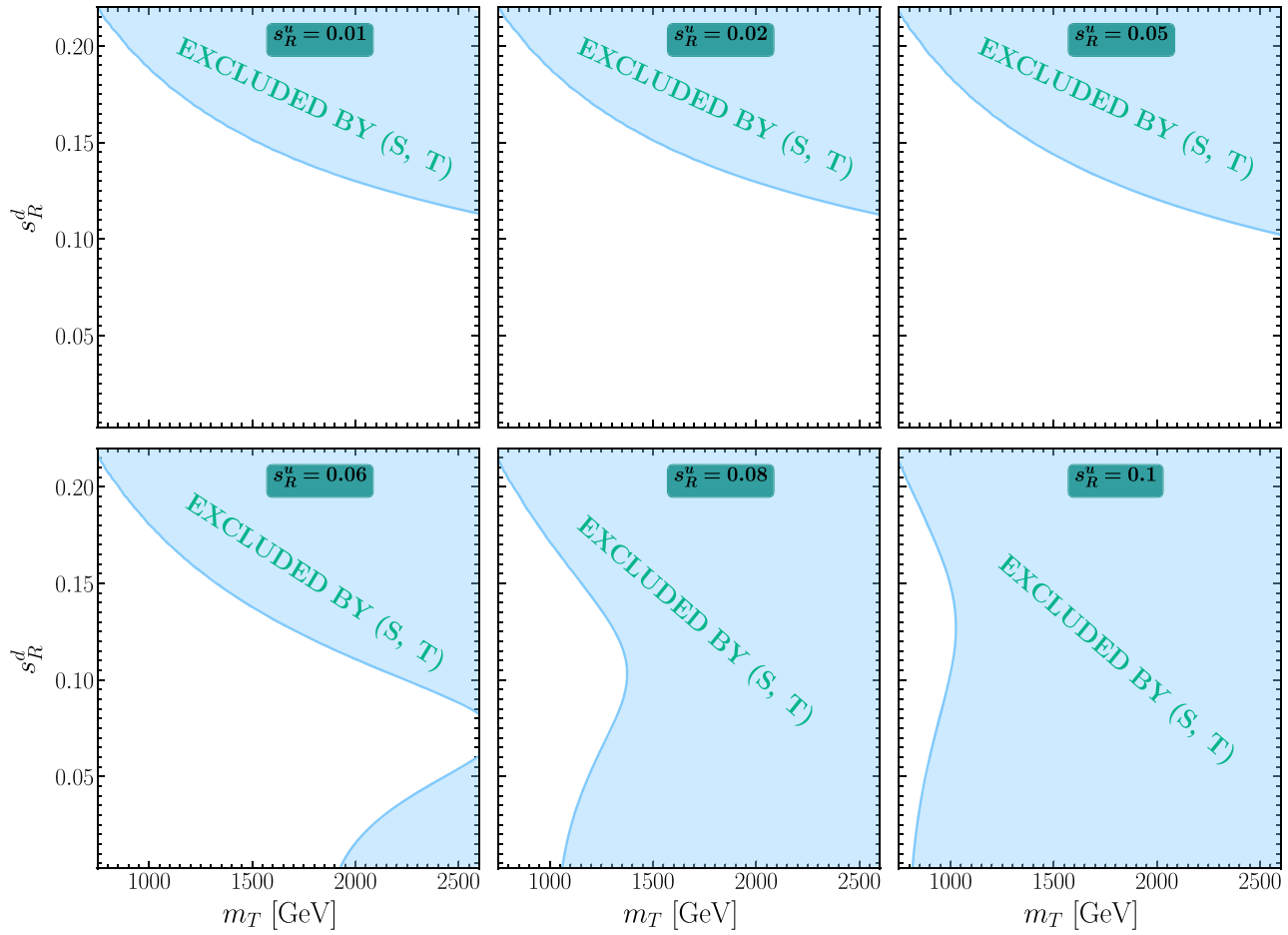

FIG. 8. Exclusion regions by (S, T) in the (m_T, s_R^d) plane for various values of s_R^u, with fixed parameters: $m_H = 532.80$, $m_A = 524.26$, and $m_{H^\pm} = 588.02$, with $\tan\beta = 5.19$.

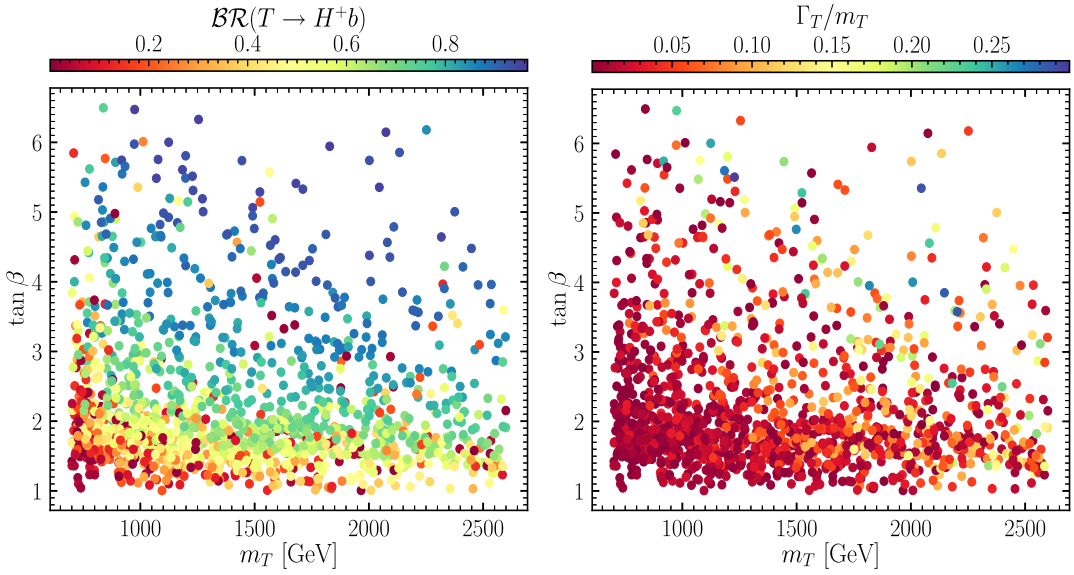

FIG. 9. $\mathcal{BR}(T \to H^+ b)$ (left) and Γ_T/m_T (right) plotted over the $(m_T, \tan\beta)$ plane. Results are presented for the 2HDM-II + (TB).

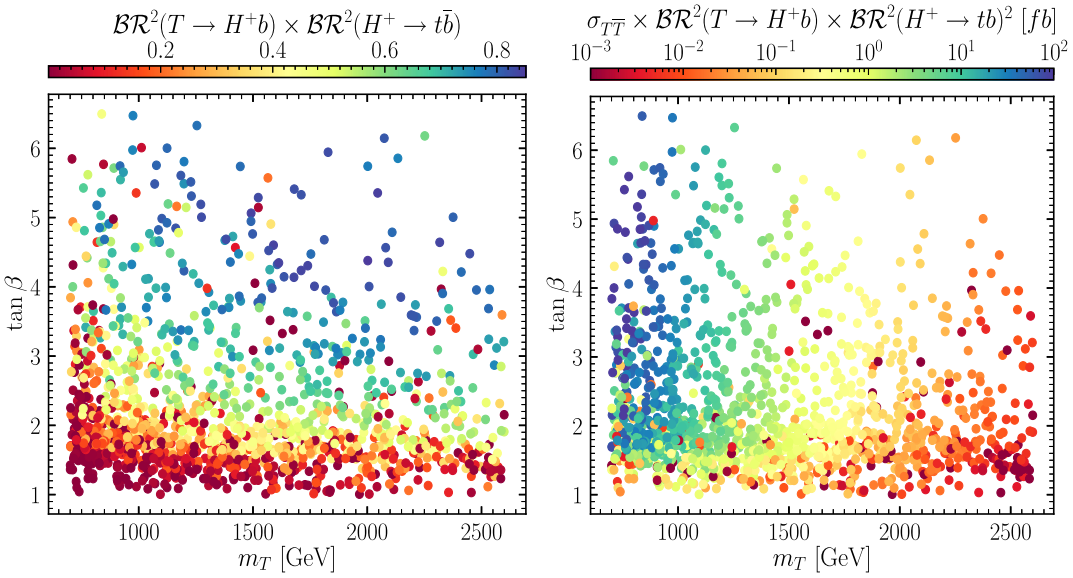

FIG. 10. $\mathcal{BR}^2(T \to H^+b) \times \mathcal{BR}^2(H^+ \to tb)$ (left) and $\sigma_{T\bar{T}} \times \mathcal{BR}^2(T \to H^+b) \times \mathcal{BR}^2(H^+ \to tb)$ (right) plotted over the $(m_T, \tan\beta)$ plane. Results are presented for the 2HDM-II + (TB).

TABLE IV. The full description of our BPs. Masses are in GeV.

	2HDM-II + (TB)		
Parameters	BP_1	BP_2	BP_3
m_h	125.00	125.00	125.00
m_H	425.91	572.13	532.80
m_A	414.07	568.50	524.26
$m_{H^\pm}$	448.66	546.59	588.02
$\tan\beta$	4.85	6.00	5.19
m_T	828.66	1123.98	1271.68
m_B	841.84	1137.92	1282.16
s_u^L	−0.0201	−0.0089	0.0018
s_d^L	−0.0011	−0.0007	0.0005
s_R^u	−0.0964	−0.0579	0.0129
s_R^d	−0.1992	−0.1660	0.1283
$\mathcal{BR}(H^\pm \to XY)$ in %			
$\mathcal{BR}(H^+ \to t\bar{b})$	96.97	93.83	96.17
$\mathcal{BR}(T \to XY)$ in %			
$\mathcal{BR}(T \to W^+b)$	7.74	4.53	5.66
$\mathcal{BR}(T \to Zt)$	0.79	0.26	0.03
$\mathcal{BR}(T \to ht)$	1.04	0.30	0.03
$\mathcal{BR}(T \to H^+b)$	90.43	94.92	94.28
Γ in GeV			
$\Gamma(T)$	95.64	283.32	196.11
σ (fb)			
$\sigma_{T\bar{T}} \times \mathcal{BR}^2(T \to H^+b) \times \mathcal{BR}^2(H^+ \to t\bar{b})$	99.86	14.09	6.22

approximately 360 GeV, compared to the typical 580 GeV in the 2HDM-II.

Furthermore, we observed a remarkable distinction between the 2HDM-II + (TB) and 2HDM-II + (T) representations. The former exhibits a substantial production rate of charged Higgs bosons, approaching nearly 100%, while the latter achieves only 25%, in terms of the $\mathcal{BR}(T \to H^+b)$. Our study thus further delved into the pair production of T $(pp \to T\bar{T})$, followed by the decays $T \to H^\pm b$ of both VLQs. In both scenarios, the charged Higgs boson subsequently undergoes decay into tb, yielding a distinctive final state characterized by two top and four bottom quarks ($2t4b$). Notably, our results indicate that this signal can reach 100 fb in the 2HDM-II + (TB), whereas for the 2HDM-II + (T) case, the corresponding rates are significantly smaller, so as to be of little relevance for the forthcoming LHC runs. Hence, we finally produced three BPs in the 2HDM-II + (TB) amenable to experimental investigation.

While a comprehensive analysis of $H^\pm$ decays has not been performed in this study, we are confident that the $H^\pm \to tb$ channel ($2t4b$ final state) from $T\bar{T}$ production and decay is a promising avenue for further exploration. This endeavor, most likely during run 3 and certainly at the High Luminosity LHC, awaits a future publication where a detailed analysis of $H^\pm$ decay channels will be performed.

ACKNOWLEDGMENTS

S. M. is supported in part through the NExT Institute and the STFC Consolidated Grant No. ST/L000296/1. We thank Rikard Enberg for many fruitful discussions.

APPENDIX A: CHARGED HIGGS BOSON COUPLINGS

In this section, we provide further elaboration on the charged Higgs couplings within the 2HDM-II + (T) and 2HDM-II + (TB) frameworks.

1. 2HDM-II + (T)

The Yukawa Lagrangian of the 2HDM-II + (T) can be expressed as[9]

$$\begin{aligned}\mathcal{L}_Y = &-y^u_{ij}\bar{Q}^0_{Li}\tilde{\Phi}_2 u^0_{Rj} + y^d_{ij}\bar{Q}^0_{Li}\Phi_1 d^0_{Rj} \\ &- y^u_{i4}\bar{Q}^0_{Li}\tilde{\Phi}_2 u^0_{R4} + \text{H.c.},\end{aligned} \tag{A1}$$

where $\Phi_{1,2}$ are the Higgs doublets, $\tilde{\Phi}_i \equiv i\sigma_2\Phi_i^*$, $\bar{Q}^0_{Li} = (\bar{u}^0_{Li} \quad \bar{d}^0_{Li})$ is the weak isospin quark doublet, and u^0_{Rj}, u^0_{R4} and d^0_{Rj} are weak isospin quark singlets.

Assuming that the new VLQs predominantly mix with the third generation (i, $j = 3$), we can express this as

$$\begin{aligned}\mathcal{L}_Y = &-y^u_{33}\begin{pmatrix}\bar{u}^0_{L3} & \bar{d}^0_{L3}\end{pmatrix}\begin{pmatrix}\frac{1}{\sqrt{2}}\left[\cos\alpha h + \sin\alpha H - i(\sin\beta G^0 + \cos\beta A)\right] \\ -(\sin\beta G^+ + \cos\beta H^+)\end{pmatrix}u^0_{R3} \\ &- y^u_{34}\begin{pmatrix}\bar{u}^0_{L3} & \bar{d}^0_{L3}\end{pmatrix}\begin{pmatrix}\frac{1}{\sqrt{2}}\left[\cos\alpha h + \sin\alpha H - i(\sin\beta G^0 + \cos\beta A)\right] \\ -(\sin\beta G^+ + \cos\beta H^+)\end{pmatrix}u^0_{R4} \\ &+ y^d_{33}\begin{pmatrix}\bar{u}^0_{L3} & \bar{d}^0_{L3}\end{pmatrix}\begin{pmatrix}-\cos\beta G^- + \sin\beta H^- \\ -\frac{1}{\sqrt{2}}\left[-\sin\alpha h + \cos\alpha H + i(\cos\beta G^0 - \sin\beta A)\right]\end{pmatrix}d^0_{R3} + \text{H.c.}\end{aligned} \tag{A2}$$

Let us focus on the charged Higgs boson $H^\pm$:

$$\begin{aligned}\mathcal{L}_Y &\supset y^u_{33}\begin{pmatrix}\bar{u}^0_{L3} & \bar{d}^0_{L3}\end{pmatrix}\begin{pmatrix}0 \\ \cos\beta H^\pm\end{pmatrix}u^0_{R3} + y^u_{34}\begin{pmatrix}\bar{u}^0_{L3} & \bar{d}^0_{L3}\end{pmatrix}\begin{pmatrix}0 \\ \cos\beta H^\pm\end{pmatrix}u^0_{R4} + y^d_{33}\begin{pmatrix}\bar{u}^0_{L3} & \bar{d}^0_{L3}\end{pmatrix}\begin{pmatrix}\sin\beta H^\pm \\ 0\end{pmatrix}d^0_{R3} \\ &\supset y^u_{33}\bar{d}^0_{L3}u^0_{R3}\cos\beta H^\pm + y^u_{34}\bar{d}^0_{L3}u^0_{R4}\cos\beta H^\pm + y^d_{33}\bar{u}^0_{L3}d^0_{R3}\sin\beta H^\pm\end{aligned} \tag{A3}$$

$$\mathcal{L}_Y = \begin{pmatrix}\bar{d}^0_{L3} & \bar{d}^0_{L4}\end{pmatrix}\underbrace{\begin{pmatrix}y^{u\,*}_{33} & y^{u\,*}_{34} \\ 0 & 0\end{pmatrix}}_{(*)}\begin{pmatrix}\bar{u}^0_{R3} \\ \bar{u}^0_{R4}\end{pmatrix}\cos\beta H^\pm + y^d_{33}\begin{pmatrix}\bar{u}^0_{L3} & \bar{u}^0_{L4}\end{pmatrix}\begin{pmatrix}d^0_{R3} \\ d^0_{R4}\end{pmatrix}\sin\beta H^\pm. \tag{A4}$$

Given our assumption that the new VLQs primarily mix with the third generation, we can write

$$\begin{pmatrix}u_{L3,R3} \\ u_{L4,R4}\end{pmatrix} = U^u_{L,R}\begin{pmatrix}u^0_{L3,R3} \\ u^0_{L4,R4}\end{pmatrix} = \begin{pmatrix}c^u_{L,R} & -s^u_{L,R}e^{i\phi_u} \\ s^u_{L,R}e^{-i\phi_u} & c^u_{L,R}\end{pmatrix}\begin{pmatrix}u^0_{L3,R3} \\ u^0_{L4,R4}\end{pmatrix}. \tag{A5}$$

Now, let us express $(*)$ in the form of the mass matrix $\mathcal{M}^u$:

$$\begin{pmatrix}y^{u\,*}_{33} & y^{u\,*}_{34} \\ 0 & 0\end{pmatrix} = \frac{\sqrt{2}}{v}\underbrace{\begin{pmatrix}1 & 0 \\ 0 & 0\end{pmatrix}}_{Y^0}\underbrace{\begin{pmatrix}y^u_{33}\frac{v}{\sqrt{2}} & y^u_{34}\frac{v}{\sqrt{2}} \\ 0 & M^0\end{pmatrix}}_{\mathcal{M}^u}. \tag{A6}$$

Consequently, Eq. (A4) can be formulated as

$$\begin{aligned}\mathcal{L}_Y &= \frac{\sqrt{2}}{v}\left[\begin{pmatrix}\bar{d}_{L3} & \bar{d}_{L4}\end{pmatrix}U^d_L Y^0 U^{u\,\dagger}_L \underbrace{U^u_L \mathcal{M}^u U^{u\,\dagger}_R}_{\mathcal{M}^u_{\text{diag}}} U^u_R U^{u\,\dagger}_R \begin{pmatrix}u_{R3} \\ u_{R4}\end{pmatrix}\cos\beta + m_b\left(c^u_L\bar{u}_{L3}d_{R3} + s^u_L\bar{u}_{L4}d_{R3}\right)\sin\beta\right]H^\pm \\ &= \frac{\sqrt{2}}{v}\left[\begin{pmatrix}\bar{d}_{L3} & \bar{d}_{L4}\end{pmatrix}\begin{pmatrix}m_t c^u_L & m_T s^u_L \\ 0 & 0\end{pmatrix}\begin{pmatrix}u_{R3} \\ u_{R4}\end{pmatrix}\cos\beta + m_b\left(c^u_L\bar{u}_{L3}d_{R3} + s^u_L\bar{u}_{L4}d_{R3}\right)\sin\beta\right]H^\pm.\end{aligned} \tag{A7}$$

[9]Note that in the 2HDM-II, $\Phi_1 = \begin{pmatrix}H^-_d \\ -H^0_d\end{pmatrix}$ couples to down quarks and $\Phi_2 = \begin{pmatrix}H^0_u \\ -H^+_u\end{pmatrix}$ couples to up quarks.

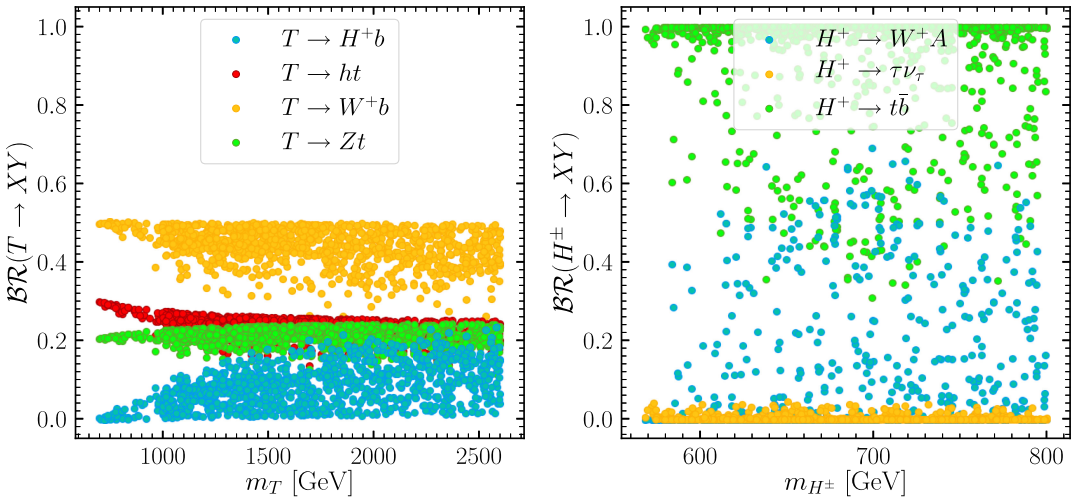

FIG. 11. Left: $\mathcal{BR}(T \to XY)$ as a function of m_T, with $XY = H^+ b$ blue, ht red, $W^+ b$ yellow and Zt green. Right: $\mathcal{BR}(H^\pm \to XY)$ as a function of $m_{H^\pm}$, with $XY = W^+ A$ blue, $\tau\nu$ yellow, and tb green; for 2HDM-II + (T).

Subsequently, we obtain

$$H^\pm tb = -\frac{g}{\sqrt{2}M_W \sin\beta} m_t c_L^u \cos\beta - \frac{g}{\sqrt{2}M_W \cos\beta} m_b c_L^u \sin\beta$$
$$= -\frac{g m_t}{\sqrt{2}M_W}\left[c_L^u \cot\beta + \frac{m_b}{m_t} c_L^u \tan\beta\right] \quad \text{(A8)}$$

$$H^\pm Tb = -\frac{g}{\sqrt{2}M_W \sin\beta} m_T s_L^u \cos\beta - \frac{g}{\sqrt{2}M_W \cos\beta} m_b s_L^u \sin\beta$$
$$= -\frac{g m_T}{\sqrt{2}M_W}\left[s_L^u \cot\beta + \frac{m_b}{m_T} s_L^u \tan\beta\right]. \quad \text{(A9)}$$

Hence,

$$Z_L^{tb} = c_L^u \quad Z_R^{tb} = \frac{m_b}{m_t} c_L^u$$
$$Z_L^{Tb} = s_L^u \quad Z_R^{Tb} = \frac{m_b}{m_T} s_L^u. \quad \text{(A10)}$$

In Fig. 11, the $\mathcal{BR}$s of T and $H^\pm$ in the 2HDM-II + (T) scenario are illustrated as functions of their respective masses. The left panel indicates that the $\mathcal{BR}(T \to H^+ b)$ can reach a maximum of 25% for $m_T > 2000$ GeV. This limitation is due to the coupling depicted earlier, which is proportional to the mixing angle s_L^u, a parameter constrained to be very small by the oblique parameters S and T. Shifting to the right panel, clearly we can see that the charged Higgs boson predominantly decays through the fermionic channel $H^+ \to t\bar{b}$ achieving approximately 100% across the entire range of charged Higgs masses.

2. 2HDM-II + (TB)

The Yukawa Lagrangian for the doublet (TB) case can be expressed as

$$\mathcal{L}_Y = -y_{ij}^u \bar{Q}_{Li,j,4}^0 \tilde{\Phi}_2 u_{Rj}^0 + y_{ij}^d \bar{Q}_{Li,j,4}^0 \Phi_1 d_{Rj}^0$$
$$- y_{4j}^u \bar{Q}_{Li,j,4}^0 \tilde{\Phi}_2 u_{R4}^0 + y_{4j}^d \bar{Q}_{Li,j,4}^0 \Phi_1 d_{R4}^0 + \text{H.c.} \quad \text{(A11)}$$

Following the same steps as in the previous scenario, we can express the charged Higgs Yukawa Lagrangian as

$$\mathcal{L}_{H^\pm} = \begin{pmatrix} \bar{u}_{L3}^0 & \bar{u}_{L4}^0 \end{pmatrix} \underbrace{\begin{pmatrix} y_{33}^d & 0 \\ y_{43}^d & 0 \end{pmatrix}}_{*} \begin{pmatrix} d_{R3}^0 \\ d_{R4}^0 \end{pmatrix} \sin\beta H^\pm$$
$$+ \begin{pmatrix} \bar{d}_{L3}^0 & \bar{d}_{L4}^0 \end{pmatrix} \underbrace{\begin{pmatrix} y_{33}^u & 0 \\ y_{43}^u & 0 \end{pmatrix}}_{**} \begin{pmatrix} u_{R3}^0 \\ u_{R4}^0 \end{pmatrix} \cos\beta H^\pm. \quad \text{(A12)}$$

Now, let us express $(*)$ and $(**)$ in the form of the mass matrices $\mathcal{M}^u$ and $\mathcal{M}^d$:

$$\begin{pmatrix} y_{33}^d & 0 \\ y_{43}^d & 0 \end{pmatrix} = \frac{\sqrt{2}}{v} \underbrace{\begin{pmatrix} y_{33}^d \frac{v}{\sqrt{2}} & 0 \\ y_{43}^d \frac{v}{\sqrt{2}} & M^0 \end{pmatrix}}_{\mathcal{M}^d} \underbrace{\begin{pmatrix} 1 & 0 \\ 0 & 0 \end{pmatrix}}_{Y^0} \quad \text{(A13)}$$

$$\begin{pmatrix} y_{33}^u & 0 \\ y_{43}^u & 0 \end{pmatrix} = \frac{\sqrt{2}}{v} \underbrace{\begin{pmatrix} y_{33}^u \frac{v}{\sqrt{2}} & 0 \\ y_{43}^u \frac{v}{\sqrt{2}} & M^0 \end{pmatrix}}_{\mathcal{M}^u} \underbrace{\begin{pmatrix} 1 & 0 \\ 0 & 0 \end{pmatrix}}_{Y^0}. \quad \text{(A14)}$$

Then Eq. (A12) can be written as

$$
\begin{aligned}
\mathcal{L}_{H^\pm} &= \frac{\sqrt{2}}{v}\left[\begin{pmatrix}\bar{u}^0_{L3} & \bar{u}^0_{L4}\end{pmatrix}\mathcal{M}^d Y^0\begin{pmatrix}d^0_{R3}\\ d^0_{R4}\end{pmatrix}\sin\beta + \begin{pmatrix}\bar{d}^0_{L3} & \bar{d}^0_{L4}\end{pmatrix}\mathcal{M}^u Y^0\begin{pmatrix}u^0_{R3}\\ u^0_{R4}\end{pmatrix}\cos\beta\right]H^\pm \\
&= \frac{\sqrt{2}}{v}\left[\begin{pmatrix}\bar{u}_{L3} & \bar{u}_{L4}\end{pmatrix}U^u_L U^{d\dagger}_L \underbrace{U^u_L \mathcal{M}^u U^{u\dagger}_R}_{\mathcal{M}^d_{\rm diag}} U^d_R Y^0 U^{d\dagger}_R\begin{pmatrix}d_{R3}\\ d_{R4}\end{pmatrix}\sin\beta\right. \\
&\quad \left. + \begin{pmatrix}\bar{d}_{L3} & \bar{d}_{L4}\end{pmatrix}U^d_L U^{u\dagger}_L \underbrace{U^u_L \mathcal{M}^u U^{u\dagger}_R}_{\mathcal{M}^u_{\rm diag}} U^u_R Y^0 U^{u\dagger}_R\begin{pmatrix}u_{R3}\\ u_{R4}\end{pmatrix}\cos\beta\right]H^\pm \\
&= \frac{\sqrt{2}}{v}\left[\begin{pmatrix}\bar{u}_{L3} & \bar{u}_{L4}\end{pmatrix}\underbrace{\begin{pmatrix}c^u_L c^d_L + s^u_L s^d_L & c^u_L s^d_L - s^u_L c^d_L\\ s^u_L c^d_L - c^u_L s^d_L & s^u_L s^d_L + c^u_L c^d_L\end{pmatrix}\begin{pmatrix}c^{d\,2}_R m_b & s^d_R c^d_R m_b\\ s^d_R c^d_R m_B & s^{d\,2}_R m_B\end{pmatrix}}_{\mathcal{M}_1}\begin{pmatrix}d_{R3}\\ d_{R4}\end{pmatrix}\sin\beta\right. \\
&\quad \left. + \begin{pmatrix}\bar{d}_{L3} & \bar{d}_{L4}\end{pmatrix}\underbrace{\begin{pmatrix}c^d_L c^u_L + s^d_L s^u_L & c^d_L s^u_L - s^d_L c^u_L\\ s^d_L c^u_L - c^d_L s^u_L & s^d_L s^u_L + c^d_L c^u_L\end{pmatrix}\begin{pmatrix}c^{u\,2}_R m_t & s^u_R c^u_R m_t\\ s^u_R c^u_R m_T & s^{u\,2}_R m_T\end{pmatrix}}_{\mathcal{M}_2}\begin{pmatrix}u_{R3}\\ u_{R4}\end{pmatrix}\cos\beta\right]H^\pm. \qquad \text{(A15)}
\end{aligned}
$$

For the coupling of H^+tb,

$$
\begin{aligned}
H^\pm tb &= -\frac{g}{\sqrt{2}M_W\cos\beta}\sin\beta\mathcal{M}_1[1,1] - \frac{g}{\sqrt{2}M_W\sin\beta}\cos\beta\mathcal{M}_2[1,1] \\
&= -\frac{g\tan\beta}{\sqrt{2}M_W}\left[m_b c^{d\,2}_R\left(c^u_L c^d_L + s^u_L s^d_L\right) + m_B s^d_R c^d_R\left(c^u_L s^d_L - s^u_L c^d_L\right)\right] \\
&\quad -\frac{g\cot\beta}{\sqrt{2}M_W}\left[m_t c^{u\,2}_R\left(c^d_L c^u_L + s^d_L s^u_L\right) + m_T s^u_R c^u_R\left(c^d_L s^u_L - s^d_L c^u_L\right)\right], \qquad \text{(A16)}
\end{aligned}
$$

we use

$$
c^{u,d}_R = \frac{m_q}{m_Q}\frac{c^{u,d}_L}{s^{u,d}_L}s^{u,d}_R, \qquad \text{(A17)}
$$

we get

$$
H^\pm tb = -\frac{g m_t}{\sqrt{2}M_W}\left[c^d_L c^u_L + \frac{s^d_L}{s^u_L}\left(s^{u\,2}_L - s^{u\,2}_R\right)\cot\beta + \frac{m_b}{m_t}\left[c^u_L c^d_L + \frac{s^u_L}{s^d_L}\left(s^{d\,2}_L - s^{d\,2}_R\right)\right]\tan\beta\right], \qquad \text{(A18)}
$$

then we get

$$
Z^{tb}_L = c^d_L c^u_L + \frac{s^d_L}{s^u_L}\left(s^{u\,2}_L - s^{u\,2}_R\right) \qquad Z^{tb}_R = \frac{m_b}{m_t}\left[c^u_L c^d_L + \frac{s^u_L}{s^d_L}\left(s^{d\,2}_L - s^{d\,2}_R\right)\right]. \qquad \text{(A19)}
$$

For the coupling of $H^\pm Tb$,

$$
\begin{aligned}
H^\pm Tb &= -\frac{g}{\sqrt{2}M_W\cos\beta}\sin\beta\mathcal{M}_1[2,1] - \frac{g}{\sqrt{2}M_W\sin\beta}\cos\beta\mathcal{M}_2[1,2] \\
&= -\frac{g\tan\beta}{\sqrt{2}M_W}\left[m_b c^{d\,2}_R\left(s^u_L c^d_L - c^u_L s^d_L\right) + m_B s^d_R c^d_R\left(s^u_L s^d_L - c^u_L c^d_L\right)\right] \\
&\quad -\frac{g\cot\beta}{\sqrt{2}M_W}\left[m_t s^u_R c^u_R\left(c^d_L c^u_L + s^d_L s^u_L\right) + m_T s^{u\,2}_R\left(c^d_L s^u_L - s^d_L c^u_L\right)\right], \qquad \text{(A20)}
\end{aligned}
$$

we use Eq. (A17) and we get

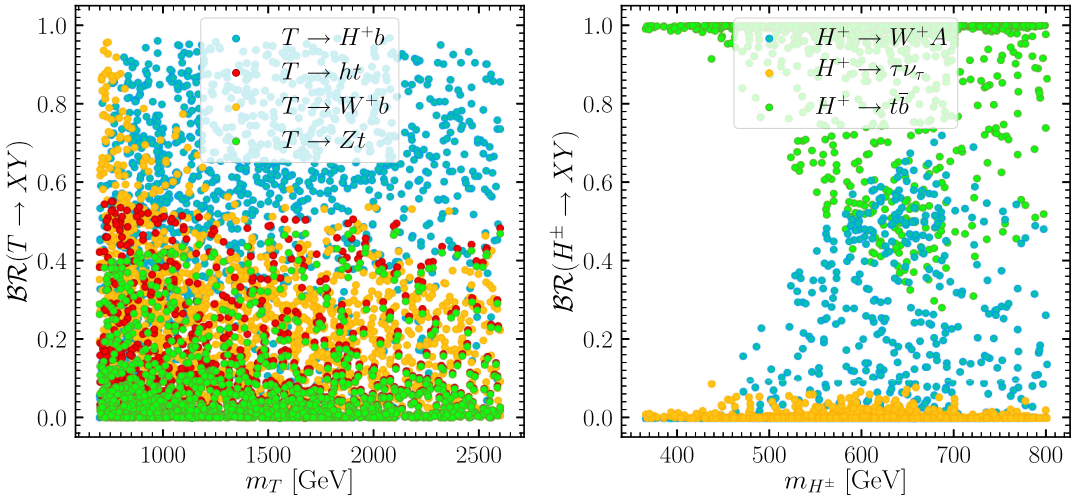

FIG. 12. The same as Fig. 11 but for 2HDM-II + (TB).

$$H^\pm Tb = -\frac{g m_t}{\sqrt{2} M_W}\left[c_L^d s_L^u + \frac{s_L^d}{c_L^u}\left(s_L^{u2} - s_R^{u2}\right)\cot\beta + \frac{m_b}{m_T}\left[c_L^d s_L^u + \frac{c_L^u}{s_L^d}\left(s_R^{d2} - s_L^{d2}\right)\right]\tan\beta\right]. \quad \text{(A21)}$$

Finally, we get

$$Z_L^{Tb} = c_L^d s_L^u + \frac{s_L^d}{c_L^u}\left(s_L^{u2} - s_R^{u2}\right)$$
$$Z_R^{Tb} = \frac{m_b}{m_T}\left[c_L^d s_L^u + \frac{c_L^u}{s_L^d}\left(s_R^{d2} - s_L^{d2}\right)\right]. \quad \text{(A22)}$$

Similar to Fig. 11, we illustrate in Fig. 12 the $\mathcal{BR}$s of T and $H^\pm$ as functions of their respective masses, but within the context of the 2HDM-II + (TB) scenario. Beginning with the left panel, in contrast to the previous scenario (2HDM-II + (T)), the production of charged Higgs from the new top quark T dominates for $m_T > 1000$ GeV, reaching nearly 100%. Shifting to the right panel, and as anticipated for heavy charged Higgs masses, the primary decay channel remains the fermionic one $H^+ \to t\bar{b}$, achieving approximately 100% $\mathcal{BR}$ across the entire range of charged Higgs masses.

APPENDIX B: LHC LIMITS ON VLQs

In this section, we evaluate the compatibility of our results with the latest LHC constraints. Figure 13 presents our data as orange points, juxtaposed with the ATLAS limits, represented by blue [89] and green [90] lines, on the (m_T, κ) plane. The coupling κ, explained further in [26,91], takes the form of $s_L^u c_L^u$ in the singlet scenario (2HDM + T) and $s_R^u c_R^u$ in the doublet scenario (2HDM+TB). Importantly, as discussed previously, the oblique parameters S and T

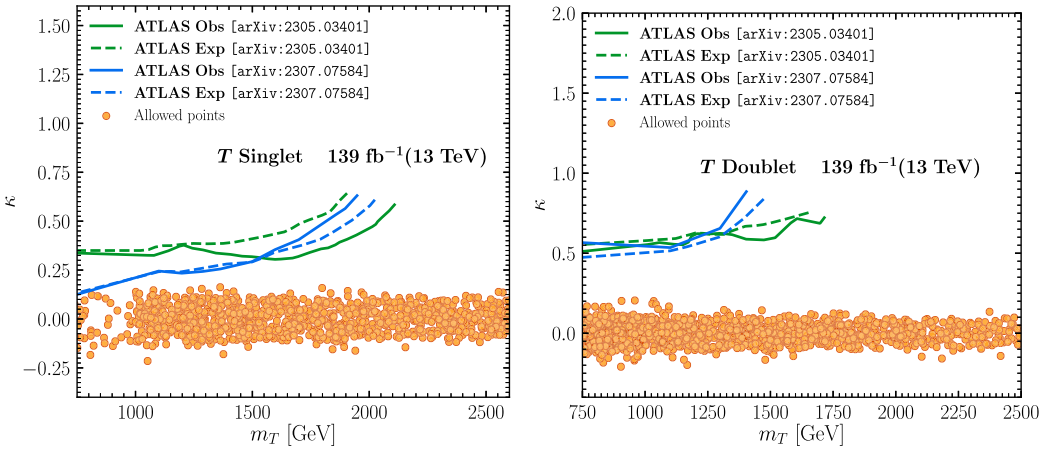

FIG. 13. Allowed points in the (m_T, κ) plane for (T) singlet (left) and (TB) doublet (right). Blue lines represent ATLAS limits [90] (solid for observed, dashed for expected), while green lines represent [89]. Notably, our analysis includes an extrapolation of these limits to expand the mass range downward to 750 GeV, considering that the original dataset commenced at ~1000 GeV.

impose stringent constraints on the mixing angles, limiting them to small values. This confinement is pivotal, ensuring our scenarios comply with the existing LHC limits and simultaneously allowing exploration of a broader VLQ mass (m_T) range.

APPENDIX C: VLQ CONTRIBUTIONS TO THE OBLIQUE PARAMETERS

Herein, we derive and present analytical and general expressions for the two VLQ representations,[10] T and TB. These expressions are formulated as functions of the scalar Passarino-Veltman functions, which are a standard in this area of study. The oblique parameters are expressed in terms of the two-point functions of the gauge bosons, as detailed below:

$$S = \frac{4s_W^2 c_W^2}{\alpha}\Re e\left[\frac{\Pi_{\gamma\gamma}(m_Z^2)}{m_Z^2} - \frac{\Pi_{ZZ}(m_Z^2)-\Pi_{ZZ}(0)}{m_Z^2} - \left(\frac{c_W^2 - s_W^2}{c_W s_W}\right)\left(\frac{\Pi_{Z\gamma}(m_Z^2)+\Pi_{Z\gamma}(0)}{m_Z^2}\right)\right] \tag{C1}$$

$$T = \frac{1}{\alpha}\Re e\left[\frac{\Pi_{ZZ}(0)}{m_Z^2} - \frac{\Pi_{WW}(0)}{m_W^2} - \frac{2s_W}{c_W}\frac{\Pi_{Z\gamma}(0)}{m_Z^2}\right] \tag{C2}$$

$$U = \frac{4s_W^2}{\alpha}\Re e\left[\frac{\Pi_{WW}(0)-\Pi_{WW}(m_W^2)}{m_W^2} - c_W^2\frac{\Pi_{ZZ}(0)-\Pi_{ZZ}(m_Z^2)}{m_Z^2} - 2s_W c_W\frac{\Pi_{\gamma Z}(0)-\Pi_{\gamma Z}(m_Z^2)}{m_Z^2} + s_W^2\frac{\Pi_{\gamma\gamma}(m_Z^2)}{m_Z^2}\right]. \tag{C3}$$

Here, α denotes the fine-structure constant, while c_W and s_W represent the cosine and sine of the Weinberg angle, respectively.

For the analytical calculations of the self-energy of gauge bosons, as depicted in Eqs. (C1) and (C2), we employ the FEYNARTS/FORMCALC public codes. These calculations specifically address scenarios where VLQs interact exclusively with third-generation SM quarks. We concentrate on the contributions from these heavy quarks, namely the SM top and bottom quarks, along with the newly introduced VLQs, since the other contributions remain the same as in the SM. With this focus, the expressions for the electroweak gauge boson self-energies can be formulated as follows:

$$-\Pi_{\gamma Z}(q^2) = \sum_f g_{\gamma z}(c^L_{Zff}, c^R_{Zff}, Q_f, m_f^2, q^2) \tag{C4}$$

$$-\Pi_{\gamma\gamma}(q^2) = \sum_f g_{VV}(Q_f, Q_f, m_f^2, m_f^2, q^2) \tag{C5}$$

$$-\Pi_{ZZ}(q^2) = 2\sum_{f_i\neq f_j}\delta_0(|Q_{f_i}-Q_{f_j}|)g_{VV} \times \left(c^L_{Zf_if_j}, c^R_{Zf_if_j}, m^2_{f_i}, m^2_{f_j}, q^2\right) + \sum_f g_{VV}\left(c^L_{Zff}, c^R_{Zff}, m_f^2, m_f^2, q^2\right) \tag{C6}$$

$$-\Pi_{WW}(q^2) = \sum_{f_i\neq f_j}\delta_1(|Q_{f_i}-Q_{f_j}|)g_{VV} \times \left(c^L_{Wf_if_j}, c^R_{Wf_if_j}, m^2_{f_i}, m^2_{f_j}, q^2\right). \tag{C7}$$

Here, c_{Vff} represents the couplings between the gauge boson Z or W and two fermions ($f = t, b, T, B$), detailed in the next Sec. C 1. The functions g_{ab}, including g_{VV} and $g_{Z\gamma}$, are defined as

$$g_{VV}(x,y,m_1^2,m_2^2,k^2) = \frac{N_c}{8\pi^2}\Big[(x^2+y^2)(A_0(m_2^2) - 2B_{00}(k^2,m_1^2,m_2^2) + k^2B_1(k^2,m_1^2,m_2^2)) + \left((x^2+y^2)m_1^2 - 2xym_1m_2\right) \times B_0(k^2,m_1^2,m_2^2)\Big] \tag{C8}$$

$$g_{\gamma z}(x,y,Q,m^2,k^2) = \frac{-N_c}{8\pi^2}\Big[(x+y)Q\big(A_0(m^2) - 2B_{00}(k^2,m^2,m^2) + k^2B_1(k^2,m^2,m^2)\big)\Big]. \tag{C9}$$

N_c represents the color factor, set at $N_c = 3$ for quarks. The functions A_0, B_0, B_{00}, and B_1 are the standard Passarino-Veltman functions.

1. Gauge interactions of VLQs

The introduction of VLQs modifies the neutral and charged current interactions. The couplings between these exotic quarks and the third-generation SM quarks, as well as the electroweak massive gauge bosons, are described as follows:

$$Zq'q = \frac{e}{2s_w c_w}\gamma^\mu\left(\kappa^L_{Zq'q}\mathbb{L} + \kappa^R_{Zq'q}\mathbb{R}\right),$$
$$Wq'q = \frac{e}{\sqrt{2}s_w}\gamma^\mu\left(\kappa^L_{Wq'q}\mathbb{L} + \kappa^R_{Wq'q}\mathbb{R}\right), \tag{C10}$$

where $\kappa^{L,R}_{Vq'q}$ are the components for both left- and right-handed couplings of the Z and W bosons. Note that these

[10] We have ensured that the oblique parameters S, T, and U are UV finite and independent of the renormalization scale μ.

couplings depend on the chosen representations of VLQs as follows:

a. (T) singlet

In the $SU(2)_L$ vectorlike singlet scenario with T, the charged current couplings $\kappa^{L,R}_{Wq'q}$ are

$$\kappa^L_{Wtb} = c^u_L, \qquad \kappa^R_{Wtb} = 0,$$
$$\kappa^L_{WTb} = s^u_L, \qquad \kappa^R_{WTb} = 0. \tag{C11}$$

The neutral current couplings $\kappa^{L,R}_{Zq'q}$ are defined as

$$\kappa^L_{Ztt} = (c^u_L)^2 - \frac{4}{3}s^2_W, \qquad \kappa^R_{Ztt} = -\frac{4}{3}s^2_W,$$
$$\kappa^L_{Zbb} = -1 + \frac{2}{3}s^2_W, \qquad \kappa^R_{Zbb} = \frac{2}{3}s^2_W,$$
$$\kappa^L_{ZTT} = (s^u_L)^2 - \frac{4}{3}s^2_W, \qquad \kappa^R_{ZTT} = -\frac{4}{3}s^2_W,$$
$$\kappa^L_{ZtT} = s^u_L c^u_L, \qquad \kappa^R_{ZtT} = 0. \tag{C12}$$

b. (TB) doublet

In the (TB) doublet scenario, the couplings of T, B, and the third-generation SM quarks with the W boson are as follows:

$$\kappa^L_{Wtb} = c^u_L c^d_L + s^u_L s^d_L, \qquad \kappa^R_{Wtb} = s^u_R s^d_R,$$
$$\kappa^L_{WTB} = c^u_L c^d_L + s^u_L s^d_L, \qquad \kappa^R_{WTB} = c^u_R c^d_R,$$
$$\kappa^L_{WTb} = s^u_L c^d_L - c^u_L s^d_L, \qquad \kappa^R_{WTb} = -c^u_R s^d_R,$$
$$\kappa^L_{WtB} = c^u_L s^d_L - s^u_L c^d_L, \qquad \kappa^R_{WtB} = -s^u_R c^d_R. \tag{C13}$$

The neutral current couplings to the Z boson are expressed as

$$\kappa^L_{Ztt} = 1 - \frac{4}{3}s^2_W, \qquad \kappa^R_{Ztt} = (s^u_R)^2 - \frac{4}{3}s^2_W,$$
$$\kappa^L_{Zbb} = -1 + \frac{2}{3}s^2_W, \qquad \kappa^R_{Zbb} = -(s^d_R)^2 + \frac{2}{3}s^2_W,$$
$$\kappa^L_{ZTT} = 1 - \frac{4}{3}s^2_W, \qquad \kappa^R_{ZTT} = (c^u_R)^2 - \frac{4}{3}s^2_W,$$
$$\kappa^L_{ZBB} = -1 + \frac{2}{3}s^2_W, \qquad \kappa^R_{ZBB} = -(c^d_R)^2 + \frac{2}{3}s^2_W,$$
$$\kappa^L_{ZtT} = 0, \qquad \kappa^R_{ZtT} = -s^u_R c^u_R,$$
$$\kappa^L_{ZbB} = 0, \qquad \kappa^R_{ZbB} = s^d_R c^d_R. \tag{C14}$$

2. Passarino-Veltman functions

The Passarino-Veltman functions are defined as follows:

$$A_0(m_1^2) = \frac{(2\pi\mu)^{4-D}}{i\pi^2}\int d^D q \frac{1}{d_1}, \tag{C15}$$

$$B_0; B^\mu; B^{\mu\nu}(p_1^2, m_1^2, m_2^2) = \frac{(2\pi\mu)^{4-D}}{i\pi^2}\int d^D q \frac{1; q^\mu; q^\mu q^\nu}{d_1 d_2}. \tag{C16}$$

The denominators d_i are defined by $d_1 = q^2 - m_1^2$ and $d_2 = (q + p_1)^2 - m_2^2$, with μ being the renormalization scale. p_1 represents the external momentum, and q is the internal momentum which is integrated out.

The functions B^μ and $B^{\mu\nu}$ are decomposed as

$$B^\mu = p_1^\mu B_1, \qquad B^{\mu\nu} = g^{\mu\nu} B_{00} + p_1^\mu p_1^\nu B_{11}. \tag{C17}$$

The functions B_{00} and B_1 can be calculated by contracting B^μ and $B^{\mu\nu}$ with p_1 and $g_{\mu\nu}$, respectively:

$$B_1(p^2, m_1^2, m_2^2) = \frac{1}{2}\left[A_0(m_1^2) - A_0(m_2^2) - (p^2 + m_1^2 - m_2^2) \times B_0(p^2, m_1^2, m_2^2)\right] \tag{C18}$$

$$B_{00}(p^2, m_1^2, m_2^2) = -\frac{p^2 - 3(m_1^2 + m_2^2)}{18} + \frac{m_1^2 B_0(p^2, m_1^2, m_2^2)}{3} + \frac{A_0(m_2^2) + (p^2 + m_1^2 - m_2^2)B_1(p^2, m_1^2, m_2^2)}{6}. \tag{C19}$$

[1] A. Davidson and K. C. Wali, Family mass hierarchy from universal seesaw mechanism, Phys. Rev. Lett. **60**, 1813 (1988).

[2] K. S. Babu and R. N. Mohapatra, A solution to the strong CP problem without an axion, Phys. Rev. D **41**, 1286 (1990).

[3] B. Grinstein, M. Redi, and G. Villadoro, Low scale flavor gauge symmetries, J. High Energy Phys. 11 (2010) 067.

[4] D. Guadagnoli, R. N. Mohapatra, and I. Sung, Gauged flavor group with left-right symmetry, J. High Energy Phys. 04 (2011) 093.

[5] T. Moroi and Y. Okada, Radiative corrections to Higgs masses in the supersymmetric model with an extra family and antifamily, Mod. Phys. Lett. A **07**, 187 (1992).
[6] T. Moroi and Y. Okada, Upper bound of the lightest neutral Higgs mass in extended supersymmetric standard models, Phys. Lett. B **295**, 73 (1992).
[7] K. S. Babu, I. Gogoladze, M. U. Rehman, and Q. Shafi, Higgs boson mass, sparticle spectrum and little hierarchy problem in extended MSSM, Phys. Rev. D **78**, 055017 (2008).
[8] S. P. Martin, Extra vectorlike matter and the lightest Higgs scalar boson mass in low-energy supersymmetry, Phys. Rev. D **81**, 035004 (2010).
[9] P. W. Graham, A. Ismail, S. Rajendran, and P. Saraswat, A little solution to the little hierarchy problem: A vectorlike generation, Phys. Rev. D **81**, 055016 (2010).
[10] S. P. Martin, Raising the Higgs mass with Yukawa couplings for isotriplets in vectorlike extensions of minimal supersymmetry, Phys. Rev. D **82**, 055019 (2010).
[11] J. L. Rosner, E_6 and exotic fermions, Comments Nucl. Part. Phys. **15**, 195 (1986).
[12] R. W. Robinett, On the mixing and production of exotic fermions in E6, Phys. Rev. D **33**, 1908 (1986).
[13] N. Arkani-Hamed, A. G. Cohen, E. Katz, and A. E. Nelson, The littlest Higgs, J. High Energy Phys. 07 (2002) 034.
[14] M. Schmaltz and D. Tucker-Smith, Little Higgs review, Annu. Rev. Nucl. Part. Sci. **55**, 229 (2005).
[15] B. A. Dobrescu and C. T. Hill, Electroweak symmetry breaking via top condensation seesaw, Phys. Rev. Lett. **81**, 2634 (1998).
[16] R. S. Chivukula, B. A. Dobrescu, H. Georgi, and C. T. Hill, Top quark seesaw theory of electroweak symmetry breaking, Phys. Rev. D **59**, 075003 (1999).
[17] H.-J. He, C. T. Hill, and T. M. P. Tait, Top quark seesaw, vacuum structure and electroweak precision constraints, Phys. Rev. D **65**, 055006 (2002).
[18] C. T. Hill and E. H. Simmons, Strong dynamics and electroweak symmetry breaking, Phys. Rep. **381**, 235 (2003).
[19] K. Agashe, R. Contino, and A. Pomarol, The minimal composite Higgs model, Nucl. Phys. **B719**, 165 (2005).
[20] R. Contino, L. Da Rold, and A. Pomarol, Light custodians in natural composite Higgs models, Phys. Rev. D **75**, 055014 (2007).
[21] R. Barbieri, B. Bellazzini, V. S. Rychkov, and A. Varagnolo, The Higgs boson from an extended symmetry, Phys. Rev. D **76**, 115008 (2007).
[22] C. Anastasiou, E. Furlan, and J. Santiago, Realistic composite Higgs models, Phys. Rev. D **79**, 075003 (2009).
[23] J. A. Aguilar-Saavedra, Identifying top partners at LHC, J. High Energy Phys. 11 (2009) 030.
[24] Y. Okada and L. Panizzi, LHC signatures of vector-like quarks, Adv. High Energy Phys. **2013**, 364936 (2013).
[25] A. De Simone, O. Matsedonskyi, R. Rattazzi, and A. Wulzer, A first top partner Hunter's guide, J. High Energy Phys. 04 (2013) 004.
[26] M. Buchkremer, G. Cacciapaglia, A. Deandrea, and L. Panizzi, Model independent framework for searches of top partners, Nucl. Phys. **B876**, 376 (2013).
[27] J. A. Aguilar-Saavedra, R. Benbrik, S. Heinemeyer, and M. Pérez-Victoria, Handbook of vectorlike quarks: Mixing and single production, Phys. Rev. D **88**, 094010 (2013).
[28] ATLAS Collaboration, Search for pair production of vector-like top quarks in events with one lepton, jets, and missing transverse momentum in $\sqrt{s} = 13$ TeV pp collisions with the ATLAS detector, J. High Energy Phys. 08 (2017) 052.
[29] ATLAS Collaboration, Search for pair production of heavy vector-like quarks decaying to high-p_T W bosons and b quarks in the lepton-plus-jets final state in pp collisions at $\sqrt{s} = 13$ TeV with the ATLAS detector, J. High Energy Phys. 10 (2017) 141.
[30] ATLAS Collaboration, Search for pair production of up-type vector-like quarks and for four-top-quark events in final states with multiple b-jets with the ATLAS detector, J. High Energy Phys. 07 (2018) 089.
[31] CMS Collaboration, Search for pair production of vector-like T and B quarks in single-lepton final states using boosted jet substructure in proton-proton collisions at $\sqrt{s} = 13$ TeV, J. High Energy Phys. 11 (2017) 085.
[32] CMS Collaboration, Search for pair production of vector-like quarks in the bW$\bar{\text{b}}$W channel from proton-proton collisions at $\sqrt{s} = 13$ TeV, Phys. Lett. B **779**, 82 (2018).
[33] CMS Collaboration, Search for vector-like T and B quark pairs in final states with leptons at $\sqrt{s} = 13$ TeV, J. High Energy Phys. 08 (2018) 177.
[34] CMS Collaboration, Search for single production of a vector-like T quark decaying to a Z boson and a top quark in proton-proton collisions at $\sqrt{s} = 13$ TeV, Phys. Lett. B **781**, 574 (2018).
[35] CMS Collaboration, Search for single production of vector-like quarks decaying to a b quark and a Higgs boson, J. High Energy Phys. 06 (2018) 031.
[36] M. Aaboud *et al.* (ATLAS Collaboration), Search for single production of vector-like quarks decaying into Wb in pp collisions at $\sqrt{s} = 13$ TeV with the ATLAS detector, J. High Energy Phys. 05 (2019) 164.
[37] ATLAS Collaboration, Search for pair production of heavy vector-like quarks decaying into high-p_T W bosons and top quarks in the lepton-plus-jets final state in pp collisions at $\sqrt{s} = 13$ TeV with the ATLAS detector, J. High Energy Phys. 08 (2018) 048.
[38] ATLAS Collaboration, Search for pair production of heavy vectorlike quarks decaying into hadronic final states in pp collisions at $\sqrt{s} = 13$ TeV with the ATLAS detector, Phys. Rev. D **98**, 092005 (2018).
[39] ATLAS Collaboration, Combination of the searches for pair-produced vectorlike partners of the third-generation quarks at $\sqrt{s} = 13$ TeV with the ATLAS detector, Phys. Rev. Lett. **121**, 211801 (2018).
[40] ATLAS Collaboration, Search for single production of vector-like quarks decaying into Wb in pp collisions at $\sqrt{s} = 13$ TeV with the ATLAS detector, J. High Energy Phys. 05 (2019) 164.
[41] G. Aad *et al.* (ATLAS Collaboration), Search for single production of vector-like T quarks decaying to Ht or Zt in pp collisions at $\sqrt{s} = 13$ TeV with the ATLAS detector, J. High Energy Phys. 08 (2023) 153.
[42] G. Aad *et al.* (ATLAS Collaboration), Search for single vector-like B quark production and decay via $B \to bH(b\bar{b})$ in pp collisions at $\sqrt{s} = 13$ TeV with the ATLAS detector, J. High Energy Phys. 11 (2023) 168.

[43] G. Aad *et al.* (ATLAS Collaboration), Search for pair-production of vector-like quarks in pp collision events at $\sqrt{s} = 13 \sim$ TeV with at least one leptonically decaying Z boson and a third-generation quark with the ATLAS detector, Phys. Lett. B **843**, 138019 (2023).
[44] CMS Collaboration, Search for single production of a heavy vector-like T quark decaying to a Higgs boson and a top quark with a lepton and jets in the final state, Phys. Lett. B **771**, 80 (2017).
[45] CMS Collaboration, Search for single production of vector-like quarks decaying into a b quark and a W boson in proton-proton collisions at $\sqrt{s} = 13$ TeV, Phys. Lett. B **772**, 634 (2017).
[46] CMS Collaboration, Search for single production of vector-like quarks decaying to a top quark and a W boson in proton-proton collisions at $\sqrt{s} = 13$ TeV, Eur. Phys. J. C **79**, 90 (2019).
[47] CMS Collaboration, Search for a W' boson decaying to a vector-like quark and a top or bottom quark in the all-jets final state, J. High Energy Phys. 03 (2019) 127.
[48] A. M. Sirunyan *et al.* (CMS Collaboration), A search for bottom-type, vector-like quark pair production in a fully hadronic mode in proton-proton collisions at $\sqrt{s} = 13$ TeV, Phys. Rev. D **102**, 112004 (2020).
[49] CMS Collaboration, A search for bottom-type, vectorlike quark pair production in a fully hadronic final state in proton-proton collisions at $\sqrt{s} = 13$ TeV, Phys. Rev. D **102**, 112004 (2020).
[50] CMS Collaboration, Search for single production of a vector-like T quark decaying to a top quark and a Z boson in the final state with jets and missing transverse momentum at $\sqrt{s} = 13$ TeV, J. High Energy Phys. 05 (2022) 093.
[51] CMS Collaboration, Search for a W' boson decaying to a vector-like quark and a top or bottom quark in the all-jets final state at $\sqrt{s} = 13$ TeV, J. High Energy Phys. 09 (2022) 088.
[52] CMS Collaboration, Search for pair production of vector-like quarks in leptonic final states in proton-proton collisions at $\sqrt{s} = 13$ TeV, J. High Energy Phys. 07 (2023) 020.
[53] R. Benbrik, C.-H. Chen, and T. Nomura, Higgs singlet boson as a diphoton resonance in a vectorlike quark model, Phys. Rev. D **93**, 055034 (2016).
[54] M. Badziak, Interpreting the 750 GeV diphoton excess in minimal extensions of two-Higgs-doublet models, Phys. Lett. B **759**, 464 (2016).
[55] A. Angelescu, A. Djouadi, and G. Moreau, Scenarii for interpretations of the LHC diphoton excess: Two Higgs doublets and vector-like quarks and leptons, Phys. Lett. B **756**, 126 (2016).
[56] A. Arhrib, R. Benbrik, S. J. D. King, B. Manaut, S. Moretti, and C. S. Un, Phenomenology of 2HDM with vectorlike quarks, Phys. Rev. D **97**, 095015 (2018).
[57] R. Benbrik *et al.*, Signatures of vector-like top partners decaying into new neutral scalar or pseudoscalar bosons, J. High Energy Phys. 05 (2020) 028.
[58] G. C. Branco, P. M. Ferreira, L. Lavoura, M. N. Rebelo, M. Sher, and J. P. Silva, Theory and phenomenology of two-Higgs-doublet models, Phys. Rep. **516**, 1 (2012).
[59] J. F. Gunion, H. E. Haber, G. L. Kane, and S. Dawson, *The Higgs Hunter's Guide* (Avalon Publishing, 2000), Vol. 80.
[60] M. E. Peskin and T. Takeuchi, Estimation of oblique electroweak corrections, Phys. Rev. D **46**, 381 (1992).
[61] H. Abouabid, A. Arhrib, R. Benbrik, M. Boukidi, and J. E. Falaki, The oblique parameters in the 2HDM with vector-like quarks: Confronting M_W CDF-II anomaly, arXiv:2302.07149.
[62] G. Altarelli and R. Barbieri, Vacuum polarization effects of new physics on electroweak processes, Phys. Lett. B **253**, 161 (1991).
[63] N. Vignaroli, Z-peaked excess from heavy gluon decays to vectorlike quarks, Phys. Rev. D **91**, 115009 (2015).
[64] F. Boudjema, A. Djouadi, and C. Verzegnassi, A general sum rule for the top mass from b physics on Z resonance, Phys. Lett. B **238**, 423 (1990).
[65] S. Kanemura, T. Kubota, and E. Takasugi, Lee-Quigg-Thacker bounds for Higgs boson masses in a two doublet model, Phys. Lett. B **313**, 155 (1993).
[66] A. Barroso, P. M. Ferreira, I. P. Ivanov, and R. Santos, Metastability bounds on the two Higgs doublet model, J. High Energy Phys. 06 (2013) 045.
[67] N. G. Deshpande and E. Ma, Pattern of symmetry breaking with two Higgs doublets, Phys. Rev. D **18**, 2574 (1978).
[68] T. Hahn, Generating Feynman diagrams and amplitudes with FEYNARTS3, Comput. Phys. Commun. **140**, 418 (2001).
[69] T. Hahn and C. Schappacher, The implementation of the minimal supersymmetric standard model in FEYNARTS and FORMCALC, Comput. Phys. Commun. **143**, 54 (2002).
[70] W. Grimus, L. Lavoura, O. M. Ogreid, and P. Osland, A precision constraint on multi-Higgs-doublet models, J. Phys. G **35**, 075001 (2008).
[71] M. J. Molewski and B. J. P. Jones, Scalable qubit representations of neutrino mixing matrices, Phys. Rev. D **105**, 056024 (2022).
[72] D. Eriksson, J. Rathsman, and O. Stal, 2HDMC: Two-Higgs-doublet model calculator physics and manual, Comput. Phys. Commun. **181**, 189 (2010).
[73] P. Bechtle, D. Dercks, S. Heinemeyer, T. Klingl, T. Stefaniak, G. Weiglein, and J. Wittbrodt, HIGGSBOUNDS-5: Testing Higgs sectors in the LHC 13 TeV era, Eur. Phys. J. C **80**, 1211 (2020).
[74] P. Bechtle, S. Heinemeyer, T. Klingl, T. Stefaniak, G. Weiglein, and J. Wittbrodt, HIGGSSIGNALS-2: Probing new physics with precision Higgs measurements in the LHC 13 TeV era, Eur. Phys. J. C **81**, 145 (2021).
[75] H. Bahl, T. Biekötter, S. Heinemeyer, C. Li, S. Paasch, G. Weiglein, and J. Wittbrodt, HIGGSTOOLS: BSM scalar phenomenology with new versions of HIGGSBOUNDS and HIGGSSIGNALS, Comput. Phys. Commun. **291**, 108803 (2023).
[76] P. Bechtle, O. Brein, S. Heinemeyer, G. Weiglein, and K. E. Williams, HIGGSBOUNDS: Confronting arbitrary Higgs sectors with exclusion bounds from LEP and the Tevatron, Comput. Phys. Commun. **181**, 138 (2010).
[77] P. Bechtle, O. Brein, S. Heinemeyer, G. Weiglein, and K. E. Williams, HIGGSBOUNDS2.0.0: Confronting neutral and charged Higgs sector predictions with exclusion bounds from LEP and the Tevatron, Comput. Phys. Commun. **182**, 2605 (2011).
[78] P. Bechtle, O. Brein, S. Heinemeyer, O. Stål, T. Stefaniak, G. Weiglein, and K. E. Williams, HIGGSBOUNDS-4: Im-

proved tests of extended Higgs sectors against exclusion bounds from LEP, the Tevatron and the LHC, Eur. Phys. J. C **74**, 2693 (2014).
[79] P. Bechtle, S. Heinemeyer, O. Stal, T. Stefaniak, and G. Weiglein, Applying exclusion likelihoods from LHC searches to extended Higgs sectors, Eur. Phys. J. C **75**, 421 (2015).
[80] F. Mahmoudi, SUPERISO v2.3: A program for calculating flavor physics observables in supersymmetry, Comput. Phys. Commun. **180**, 1579 (2009).
[81] HFLAV Collaboration, Averages of b-hadron, c-hadron, and τ-lepton properties as of summer 2016, Eur. Phys. J. C **77**, 895 (2017).
[82] CMS Collaboration, Measurement of the $B_s^0 \to \mu^+\mu^-$ decay properties and search for the $B^0 \to \mu^+\mu^-$ decay in proton-proton collisions at $s = 13$ TeV, Phys. Lett. B **842**, 137955 (2023).
[83] LHCb Collaboration, Measurement of the $B_s^0 \to \mu^+\mu^-$ decay properties and search for the $B^0 \to \mu^+\mu^-$ and $B_s^0 \to \mu^+\mu^-\gamma$ decays, Phys. Rev. D **105**, 012010 (2022).
[84] LHCb Collaboration, Analysis of neutral B-meson decays into two muons, Phys. Rev. Lett. **128**, 041801 (2022).
[85] T. Hermann, M. Misiak, and M. Steinhauser, $\bar{B} \to X_s\gamma$ in the two Higgs doublet model up to next-to-next-to-leading order in QCD, J. High Energy Phys. 11 (2012) 036.
[86] J. Alwall, R. Frederix, S. Frixione, V. Hirschi, F. Maltoni, O. Mattelaer, H.-S. Shao, T. Stelzer, P. Torrielli, and M. Zaro, The automated computation of tree-level and next-to-leading order differential cross sections, and their matching to parton shower simulations, J. High Energy Phys. 07 (2014) 079.
[87] J. Pumplin, D. R. Stump, J. Huston, H. L. Lai, P. M. Nadolsky, and W. K. Tung, New generation of parton distributions with uncertainties from global QCD analysis, J. High Energy Phys. 07 (2002) 012.
[88] R. Dermisek, E. Lunghi, N. McGinnis, and S. Shin, Signals with six bottom quarks for charged and neutral Higgs bosons, J. High Energy Phys. 07 (2020) 241.
[89] ATLAS Collaboration, Search for singly produced vector-like top partners in multilepton final states with 139 fb^{-1} of pp collision data at $\sqrt{s} = 13$ TeV with the ATLAS detector, arXiv:2307.07584 [Phys. Rev. D (to be published)].
[90] ATLAS Collaboration, Search for single production of vector-like T quarks decaying into Ht or Zt in pp collisions at $\sqrt{s} = 13$ TeV with the ATLAS detector, J. High Energy Phys. 08 (2023) 153.
[91] G. Cacciapaglia, A. Deandrea, D. Harada, and Y. Okada, Bounds and decays of new heavy vector-like top partners, J. High Energy Phys. 11 (2010) 159.